LLR COMBINING FOR SHARED SPECTRUM OPERATION AND 5G WAVEFORM STUDIES

A Project Report

submitted by

VISHNU OC

in partial fulfillment of the requirements
for the award of the degree of

MASTER OF TECHNOLOGY

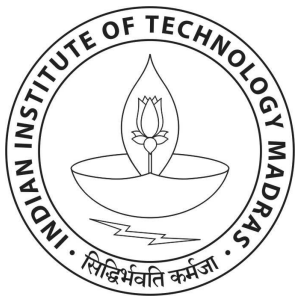

DEPARTMENT OF ELECTRICAL ENGINEERING
INDIAN INSTITUTE OF TECHNOLOGY MADRAS.

JUNE 2016

THESIS CERTIFICATE

This is to certify that the thesis titled **LLR COMBINING FOR SHARED SPECTRUM OPERATION AND 5G WAVEFORM STUDIES**, submitted by **VISHNU OC**, to the Indian Institute of Technology, Madras, for the award of the degree of **Master of Technology**, is a bona fide record of the project work done by him under my supervision. The contents of this thesis, in full or in parts, have not been submitted to any other Institute or University for the award of any degree or diploma.

Dr. K.Giridhar
(Project Guide)
Professor
Dept. of Electrical Engineering
IIT-Madras, 600 036

Place: Chennai

Date: 17^{th} June 2016

ACKNOWLEDGEMENTS

First and foremost, I am deeply indebted to my advisor Prof. K. Giridhar for his guidance and encouragement throughout the course of this project. I would like to thank him profusely for giving me an opportunity to work with him, for his patient guidance and for giving me freedom to work. His dedication and keen interest and above all, his overwhelming attitude to help his students had been solely and mainly responsible for completing my work. His timely advice, meticulous scrutiny, scholarly advice and scientific approach has helped me to a very great extent to accomplish my task.

I also thank Dr. S. Bhashyam for his valuable support as a faculty advisor during my entire tenure as a student.

It is a pleasure to thank my teammates Suman Kumar, V. Vignesh Kumar, P. Sriram, C.R. Venkatesh, M. Midhun, Umakishore G.S.V, B. Naveen Kumar, and Deepak Saidam for their help at every stage of my work. I would extend my sincere thanks to all my classmates and hostel mates for all the fun and making my stay memorable.

I take this opportunity to express my greatest regards to my family and friends for their support, co-operation and inspiration which were the sustaining factors in carrying out my work successfully.

Finally, I would like to thank the Department of Electrical Engineering and Indian Institute of Technology Madras for providing an excellent and ideal environment for learning.

ABSTRACT

In Uplink CoMP schemes as in LTE [1], usually multiple base-stations (eNodeBs) receive signals from the same user equipment (UE). Combining this information appropriately using the backhaul is known to yield high gains, especially when the interference avoidance is used across the eNodeBs in CoMP. We study a scenario where eNodeBs belonging to different operators simultaneously use the same spectrum, which may be advisable in premium but limited frequency bands available in sub-1GHz deployments. In such uplinks, if eNodeBs belonging to different operators can share LLRs, substantial performance improvement can be obtained over single-operator CoMP since the link distance between the UE and the eNodeBs of the other operators can be much less.

We propose a novel LLR computation, vector quantization and combining approach for such a spectrum shared operation. Not only does this quantized sharing approach reduce the bit rate required on the backhaul between the different eNodeBs, but also provides a performance within 0.3dB of the unquantized LLR sharing performance with only 1.2 to 2.4 bits per LLR.

We also analyse a joint Robust Log Likelihood Ratio (Robust LLR) computation for multiple UEs at a eNodeB, and combining these Robust LLRs from multiple eNodeBs to further enhance the performance. The combining technique is also applied for downlink, where LLRs are shared between device to device and 7-8 dB performance improvement is seen in the BLER performance .

As an analysis of different waveforms, we have studied and performance is analysed for multiple waveforms targeted for 5G cellular network. The waveforms considered are CP-OFDM, OFDM-WOLA, FBMC, UFMC, GFDM, DFT-s-OFDM, and ZT DFT-s-OFDM. The performance metric considered for the analysis are Peak to Average Power Ratio, Power Spectral Density,and Time-Frequency efficiency. Also, a comparison table is derived as an outcome of the detailed study of these waveforms.

TABLE OF CONTENTS

LIST OF TABLES

LIST OF FIGURES

ABBREVIATIONS

LLR	Log Likelihood Ratio
BER	Bit Error Rate
BLER	BLock Error Rate
MRC	Maximum Ratio Combining
BLC	Bit Level Combining
HARQ	Hybrid automatic repeat request
SISO	Single Input Single Output
MIMO	Multi Input Multi Output
SU-MIMO	Single User MIMO
MU-MIMO	Multi User MIMO
CG-LLR	Contaminated Gaussian LLR
CC-LLR	Contaminated Cauchy LLR
CL-LLR	Contaminated Cauchy LLR
ICI	Inter Cell Interference
CoMP	Coordinated Multi-Point
OCR	Operator Cluster Radius
UE	User Equipment
CRC	Cyclic Redundancy Check
MSE	Mean Square Error
MI	Mutual Information
SNR	Signal to Noise Ratio
SIR	Signal to Interference Ratio
PDF	Probability Distribution Function
D2D	Device To Device
OOB	Out Of Band
LTE	Long Term Evolution
LTE-A	LTE-Advanced
CP-OFDM	Cyclic Prefix-Orthogonal Frequency Division Multiplexing

OFDM-WOLA	Orthogonal Frequency Division Multiplexing-Weighted OverLapp and Add
FBMC	Filter Bank Multi Carrier
UFMC	Universal Filtered Multi Carrier
GFDM	Generalised Frequency Division Multiplexing
SC-FDM	Single Carrier-Frequency Division Multiplexing
PAPR	Peak to Average Power Ratio
PSD	Power Spectral Density

CHAPTER 1

INTRODUCTION

1.1 Introduction

In the cellular network hitherto, operators use orthogonal frequency resources. Even though multiple UEs signal arrive at the antenna port of eNodeB equipment, eNodeB hardware processes its own user signal and filters out other operator signals. In 4G, cell edge user performance is improved by using Coordinated MultiPoint(CoMP) technique [1]. The methods under CoMP are joint reception, joint transmission and joint beam forming technique [2]. These techniques do not explore the availability of other operators eNodeBs. Moreover, the cell edge user for one of the operator's eNodeB might be having good signal quality at another operator eNodeB. This is due to the spatial deployment of the eNodeBs. In this context, spectrum sharing allows us to explore all the available infrastructure to get the full benefit of the diversity gain. Another important aspect of spectrum sharing is the improvement in spectrum utilisation. In 4G, guard bands are inserted on both sides of spectrum for reducing the *Out of Band Emission*. Guard bands reduce the frequency domain efficiency to approximately 90%[3]. Consider the scenario of LTE with four operators in a cell each with 10MHz bandwidth. The number of unused subcarriers per operator is 66 and overall guard band insertion is 4$\times$ 66 subcarriers. By using shared spectrum, overall guard band requirement turns out to be 66 subcarriers, an overall reduction of 75%! So multi operator spectrum sharing is a promising technique for the futuristic cellular network where availability of orthogonal resources at various frequency bands itself is going to be a bottleneck.

In the scenario of spectrum sharing, where same spectrum is shared across multiple operators, every eNodeB receives multiple UE signals simultaneously. Performance of the cellular system can be further enhanced in uplink by sharing and processing the information judiciously. Processing can be done either

at a serving eNodeB or at a centralised node and irrespective of this location; we denote these location as serving node. Similarly in downlink all UEs receive signals from all eNodeBs. Performance in downlink can be further improved by co-operation by sharing information among UEs. The shared information can be any of the following three forms: **(i)** Digitized IQ samples and channel information, **(ii)** information bits after channel decoding, or **(iii)** LLR. By sharing IQ samples and channel information, MRC [4] scheme can be incorporated at the receiver, thereby achieving maximum capacity. However, MRC requires large backhaul (for Uplink)/D2D link (for Downlink) bandwidth. The second approach in **(ii)** of sending information bits could modestly improve the overall system performance with less backhaul/D2D link bandwidth. However, the performance improvement will be less compared to **(i)**. Method **(iii)** should lie between those two bounds, both in terms performance and backhaul/D2D link complexity. The performance bound with respect to BER or BLER will be upper bounded by **(i)** and lower bounded by **(ii)**. Backhaul/D2D Link bandwidth requirement is also bounded in the same way, and we will be targeting for the lower bound. The BLC approach described in [4] talks about a suboptimal way of LLR combining in chase combining HARQ [5] with reduced memory requirement. In our setup, the memory requirement translates into backhaul/D2D link bandwidth requirement, which will be in between the first and second method. The different tasks involved here is computing the LLRs for multiple UEs and combining these LLRs from multiple eNodeBs/UEs to achieve the spatial diversity and receive diversity gain.

Having described the requirement of decoding multiple UEs data stream, another important aspect of the work is to model the interference. In a cellular network, transmission scenario and hence the interference profile varies with frequency management/reuse schemes and carrier aggregation [6]. For example, consider the case where the cellular network is having carrier aggregation by use of Industrial, Scientific, and Medical (ISM) band and non-ISM band of frequencies. In this scenario, it is expected that one set of contiguous resources are orthogonal resources (ICI free) for the operator as compared to remaining set of resources. These interference term can be modelled as impulsive noise and considered in the LLR computation. These LLRs are usually called as Robust LLRs and performance enhancement is observed by use of this technique.

Another important candidate of improving the spectrum efficiency is to enhance the performance of the waveforms used in the cellular network. CP-OFDM modulation is a cost-effective solution for coping with large delay spread channels and has been adopted by several radio standards, from IEEE 802.11 to LTE and LTE-A [7]. The attractiveness of CP-OFDM is mainly due to its capability of converting the frequency selective channel to multiple flat channels, enabling simple one-tap equalization at the receiver. DFT-s-OFDM [8]is a straight forward add on over CP-OFDM allowing to emulate a single carrier modulation with significant advantages in terms of power efficiency. The effectiveness of both OFDM and DFT-s-OFDM in mitigating the fading is made possible through the insertion of a Cyclic Prefix (CP) at the beginning of each time symbol, obtained as a copy of the last part of the symbol itself. In case the CP length is larger than the delay spread of the channel, ISI is avoided and the signal is seen as cyclic at the receiver. This means, in the frequency domain the subcarriers where the data symbols are mapped are still orthogonal and efficient frequency domain processing can be applied.

However, the usage of the CP in an OFDM-based cellular standard leads to significant limitations in the system design. First of all, the CP length must be hard-coded in order to fit with the frame duration, which is set according to upper layer requirements (e.g., latency). For instance, in LTE two different sub frame structures have been defined: short CP of 4.7μs with 14 time symbols and long CP of 8.6 μs with 12 time symbols, both fitting the constraint of 1 ms sub frame duration. This may lead to unnecessary throughput limitations in case the effective delay spread is significantly lower than the CP duration. On the contrary, it may affect the BLER performance in case such length is not sufficiently to cope with a large delay spread. The option of using an adaptive CP, where its length is set with fine granularity according to the estimated channel, is infeasible in practical scheduled systems due to the aforementioned constraint on the fixed frame duration. Moreover, the usage of different numerologies (e.g., LTE with long CP and short CP) may strongly affect the performance of different networks operating in proximity, since they would generate mutual asynchronous interference which cannot be cancelled by computationally feasible receiver.

To avoid the above-mentioned limitations of CP-OFDM, many waveforms are getting promoted in recent year. The approaches are mainly (i) improving the spectral performance by having non-rectangular prototype filter, and (ii) improving the time domain efficiency by removing/reducing the CP duration. The different waveforms candidates are OFDM-WOLA [9], FBMC [10] [11], UFMC [12], GFDM [13], ZT DFT-s-OFDM [14]. The waveforms are usually analysed by performance metric and different performance metric are Peak to average power ratio, Out of band emission, and Time-Frequency efficiency.

1.2 Brief Overview of the Work

The overall work is broadly classified into two, i) LLR computation and combining for shared spectrum operation ii) Waveform analysis. The first part of the work is to compute the LLR for multiple UEs at a eNodeB (joint LLR computation), quantize the LLRs and combining this information appropriately using the backhaul link. This is known to yield high gains, especially when the interference avoidance is used across the EnodeBs in CoMP. We study a scenario where eNodeBs belonging to different operators simultaneously use the same spectrum, which may be advisable in premium but limited frequency bands available in sub-1GHz deployments. In such uplinks, if eNodeBs belonging to different operators can share LLRs, substantial performance improvement can be obtained over single-operator CoMP since the link distance between the UE and the eNodeBs of the other operators can be much less. The same concept is extended between devices where information is shared between UEs via wireless link instead of backhaul based eNodeB communication. Another important aspect of the work is to extend the joint LLR computation by considering the interference term into LLR generation block. Different interference scenarios are generated and analysed the performance as a part of this work. Moreover, the scheme is also applied for SISO-CoMP system as a robust multi-user detection scheme and analysed the performance.

As an analysis of different waveforms, we have studied and performance is analysed the multiple waveforms targeted for 5G cellular network. The waveforms considered are CP-OFDM, OFDM-WOLA, FBMC, UFMC, GFDM, DFT-s-OFDM,

and ZT DFT-s-OFDM. The performance metric considered for the analysis are PAPR, PSD and Time-Frequency efficiency. A comparison table is provided as an outcome of the detailed study of these waveforms.

1.3 Objective of the Work

For uplink LLR combining technique, the objective is to propose an efficient joint LLR computation method, quantization technique with minimal compromise on the BLER performance, and combining the LLRs from multiple eNodeBs. The second objective is to model the interference while computing the LLRs, these LLRs are called as Robust LLRs and analyse the Robust LLR performance for various scenarios. As an application of this method, the applicability of Robust LLR schemes to be analysed in the SISO-CoMP cellular network. The third objective is to conduct a performance analysis of the LLR combining and uniform quantization technique for D2D (Downlink) communication. The fourth objective is to carry out waveform analysis where different waveforms proposed for 5G network is to be studied and the performance analysis is to be carried out across the waveforms with respect to the performance metric.

1.4 Organization of the Thesis

Chapter 2 presents the uplink LLR combining technique for multiple UEs for the shared spectrum operation. In this chapter, a detailed system model is described, which includes envisaged cellular network and receiver details. Subsequently, we describe the method for joint LLR computation for multiple UE at eNodeB, LLR combining at the serving node and the details of cluster based quantization technique. Finally, simulation results are presented.

Chapter 3 describes robust LLR based technique for joint LLR computation for multiple UEs in the shared spectrum operation. In this chapter, we describe the system model considered where multiple scenarios will be detailed. Subsequently, we describe the noise models for interference, joint Robust LLR computation for

multiple UEs at an eNodeB, and Robust LLR combining at the serving node. Simulation results are also presented for all the scenarios considered and results are provided with misspecified values in the noise model. Finally, as an application of this method, multi-user detection scheme is presented in the SISO-CoMP context.

Chapter 4 discusses the LLR combining technique for D2D communication in a shared spectrum context. A detailed block diagram is provided and the performance result is presented in this chapter.

Chapter 5 presents the performance analysis results for various waveforms. The performance of the waveforms are analysed with respect to PAPR, PSD and Time-Frequency Efficiency. Finally, a detailed table is provided to compare all the waveforms.

Chapter 6 gives the conclusion remarks and future work.

In appendix, transmitter and receiver architecture for different waveform candidates, covering both single carrier waveforms and multicarrier waveforms, are described.

CHAPTER 2

UPLINK LLR COMPUTATION, QUANTIZATION, AND COMBINING

In 4G cellular system using 3GPP-LTE technology, cell edge user performance is improved by using Coordinated Multi Point(CoMP) technique. The methods include joint reception, joint transmission and joint beam forming technique. In our work, we desire to enhance the efficiency of Uplink CoMP by extending it to a scenario where multiple operators (say 3 to 4 operators) are allowed to simultaneously share the spectrum.

In the scenario of multiple operators sharing the same spectrum, every eNodeB receives multiple UE signals simultaneously. Performance of the cellular system can be further enhanced by sharing and processing the information judiciously. Here, we considered LLR as the shared information between eNodeBs.

2.1 System Model

We consider a 19 cell model for the analysis of the proposed technique where performance is monitored at the centre cell. A detailed sketch is given in Fig.2.1. The cell centres are separated by a constant distance, denoted here as Inter Site Distance (ISD). Each cell is equipped with four operator eNodeBs. Operators are positioned within a predetermined radius with respect to the cell centre which we denoted as Operator Cluster Radius (OCR). For the analysis purpose, various OCRs are used and it is mentioned whenever required.

It is assumed that the users belonging to various operators are uniformly distributed in the cells. The received signal at each eNodeB will be a combination of signals from its own UE, UEs belonging to the other operators from the same cell and UEs from all other cells. The received signal at the n^{th} eNodeB for any

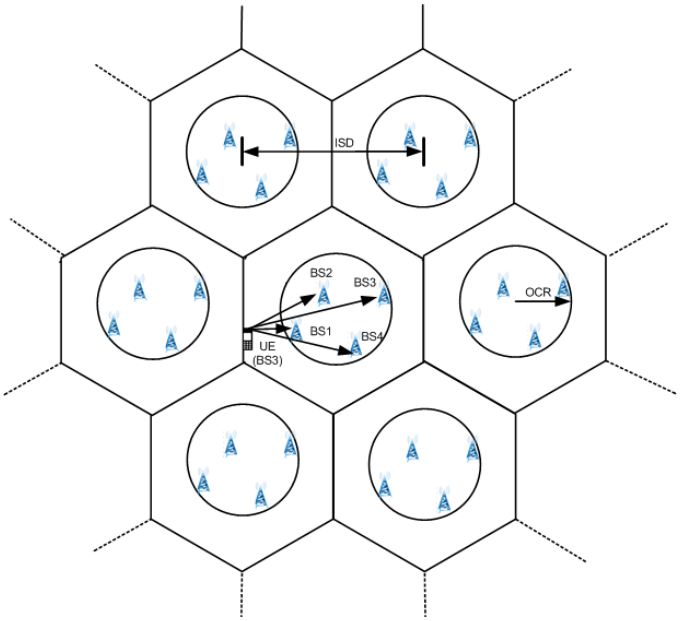

Fig. 2.1 Cellular network with four operator per cell

i^{th} time instant can be represented as follows.

$$y_n(i) = H_{1,nn}(i)x_{1,n}(i) + \underbrace{\sum_{\substack{m\in I \\ m\neq n}} H_{1,mn}(i)x_{1,m}(i)}_{\text{Modeled Interferer}} + \underbrace{\sum_{k=2}^{M}\sum_{m\in I} \psi_k H_{k,mn}(i)x_{k,m}(i)}_{\text{Unmodeled Interferer}} + n_n(i) \tag{2.1}$$

where M denotes the number of cells considered, $I = \{1, 2, 3, 4\}$ denotes the operator index, $H_{k,mn} = \sqrt{\alpha_{k,mn}\beta_{k,mn}\gamma_{k,n}}h_{k,mn}$ denote the instantaneous channel from UE of the m^{th} operator from k^{th} cell to n^{th} eNodeB. $\alpha_{k,mn}$ and $\beta_{k,mn}$ represent the path loss and shadowing fading from UE of m^{th} operator from k^{th} cell to n^{th} eNodeB respectively. Also $\gamma_{k,n}$ indicates the transmitter power of UE belonging to the n^{th} eNodeB of k^{th} cell ,which is being adjusted to get a required SNR at the serving eNodeB. The element $h_{k,mn}$ is an independent and identically distributed complex Gaussian random variable with zero mean and unit variance. $x_{k,m}(i)$'s are symbols from unit modulus constellation. $\psi_k \in \{0, 1\}$ where its value depends on frequency management scheme. For example ψ_k is one for every k in frequency-reuse one. Here, $n_n(i)$ denotes the additive complex white Gaussian noise with

zero mean and variance σ^2. Noise variance in dBm is obtained as follows

$$\sigma^2 = -174 + 10log10(BW) + NF \tag{2.2}$$

where BW indicates the receiver bandwidth in Hz and NF indicates the noise figure in dB. In the subsequent discussion, we mainly use the modelled interferers and hence k will be omitted from $H_{k,mn}$ and $x_{k,m}$ for brevity. Whenever required, it will be mentioned explicitly.

In this current study, we have assumed that the perfect channel estimate from user to all the operators eNodeB in the centre cell are available for processing. Typically channel estimate should be obtained from pilot structure and channel estimation techniques as described in [15]. In spectrum sharing scenario, orthogonal pilots can be thought about for getting a better estimate. Also, we assume that channels from user to different operator EnodeBs are independent as the eNodeBs are not co located. It is also assumed that modulation order of the modelled interferer is known for the joint LLR computation block.

An envisaged block diagram of the eNodeB hardware is shown in Fig. 2.2. The diagram which includes RF front end, ADC and Band Pass Filter, provides the IQ baseband data to the LLR computational block. LLR computational block is responsible for computing the LLR for multiple UEs based on the method described in section III. Subsequently channel decoding will be performed and checksum is extracted to verify the block error. In case of error free block, LLR combiner will be bypassed and the information bit is given for further processing. In case of Block error, LLRs will be received from other BSs on request basis. After the reception of LLR from other base stations, LLRs will be combined and given to the channel decoder for extracting information bit. The combining will be based on the quality of the LLR from different eNodeBs. LLR buffer stores the quantized LLR of UEs for different operator and sends the LLR based on the request from other eNodeBs.

A simplified block diagram of the transmitter in the UE is shown in Figure 2.3. Initially data will be segmented into multiple blocks and CRC will be appended to each segment. Subsequently Forward Error Correction coding will be performed

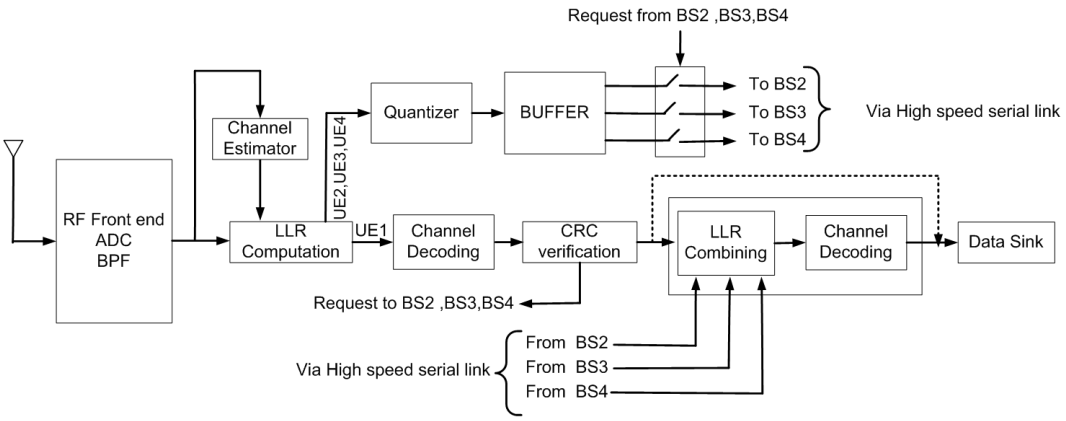

Fig. 2.2 Receiver Block Diagram

on each segment and mapped to the constellation before transmission.

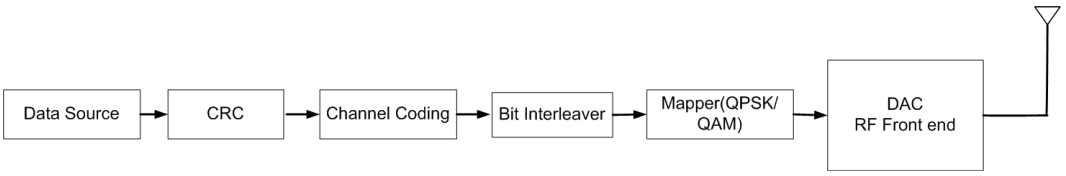

Fig. 2.3 Transmitter Block Diagram

2.2 Joint LLR Computation, Quantization, and Combining

This section describes the LLR computation technique for multiple UEs at a eNodeB, digitization of LLR of UEs belonging to different operators and combining LLRs of a UE from multiple eNodeB at serving node.

2.2.1 Joint LLR Computation

Since the received signal consists of signals from multiple UE, LLR for multiple UEs can be calculated at the eNodeB. For any time instant i, given the received signal y_i, channel from UEs to eNodeB $\underline{\mathbf{H_i}}$ and transmit symbols $\underline{\mathbf{x_i}}$, the conditional probability distribution function is defined as follows

$$Pr\{y_i|\underline{\mathbf{H_i}}, \underline{\mathbf{x_i}}\} = \frac{1}{\pi\sigma^2} \exp\{\frac{-1}{\sigma^2}\|y_i - \underline{\mathbf{H_i x_i}}\|^2\} \tag{2.3}$$

In a multi operator shared spectrum scenario, LLR is defined for all the bits of the individual UEs. LLR for λ^{th} bit of k^{th} UE is defined as,

$$LLR\_UE_{k,\lambda} = \ln \frac{Pr\{b_\lambda = 1 | y_i, \underline{\mathbf{H_i}}\}}{Pr\{b_\lambda = 0 | y_i, \underline{\mathbf{H_i}}\}} \tag{2.4}$$

where $k \in \{1, 2, 3, 4\}$, $\lambda \in \{1, 2, 3, \cdots, m_k\}$ and m_k indicates the modulation order of the k^{th} UE. By using Bayes rule, (2.4) is expanded as follows

$$LLR\_UE_{k,\lambda} = \ln \frac{Pr\{y_i | b_i = 1, \underline{\mathbf{H_i}}\} Pr\{b_i = 1\}}{Pr\{y_i | b_i = 0, \underline{\mathbf{H_i}}\} Pr\{b_i = 0\}} \tag{2.5}$$

Without loss of generality, it is assumed that prior probabilities for transmitting one and zero is the same. Then (2.5) can be written as

$$LLR\_UE_{k,\lambda} = \ln \frac{Pr\{y_i | b_i = 1, \underline{\mathbf{H_i}}\}}{Pr\{y_i | b_i = 0, \underline{\mathbf{H_i}}\}} \tag{2.6}$$

Let all the symbols for k^{th} UE belong to set X. Defining two non-overlapping sets X_0 and X_1 as follows

$$X_0 = \{x \in X | b_\lambda = 0\} \quad X_1 = \{x \in X | b_\lambda = 1\} \tag{2.7}$$

We can compute (2.6) as

$$LLR\_UE_{k,\lambda} = \ln \frac{\sum\limits_{x \in X_1} Pr\{y_i | x, \underline{\mathbf{H_i}}\}}{\sum\limits_{x \in X_0} Pr\{y_i | x, \underline{\mathbf{H_i}}\}} \tag{2.8}$$

Now by applying the conditional probability definition as per (2.3),

$$LLR\_UE_{k,\lambda} = \ln \frac{\sum\limits_{x \in X_1} \sum\limits_{\underline{s} \in I} \exp\{\frac{-1}{\sigma^2} \| y_i - H_{i,k} x - \sum_{\substack{m \in M \\ m \neq k}} H_{i,m} s_m \|^2\}}{\sum\limits_{x \in X_0} \sum\limits_{\underline{s} \in I} \exp\{\frac{-1}{\sigma^2} \| y_i - H_{i,k} x - \sum_{\substack{m \in M \\ m \neq k}} H_{i,m} s_m \|^2\}} \tag{2.9}$$

where I denote all possible symbol combination for modelled interferes and $M = \{1, 2, 3, 4\}$. For computational efficiency, jacobian algorithm [16] is used

$$\ln(e^{x_0} + e^{x_1}) = max(x_0, x_1) + \ln(1 + e^{-|x_0 - x_1|}) \tag{2.10}$$

The second term in (2.10) is a correction term for the max log approximation and

can be neglected. By using Max Log Approximation, (2.9) can be approximated as follows.

$$LLR\_UE_{k,\lambda} = \max_{x \in X_1}\{\frac{-1}{\sigma^2}\|y_i - H_{i,k}x - \sum_{\substack{m \in M \\ m \neq k}} H_{i,m}s_m\|^2\} - \max_{x \in X_0}\{\frac{-1}{\sigma^2}\|y_i - H_{i,k}x - \sum_{\substack{m \in M \\ m \neq k}} H_{i,m}s_m\|^2\} \tag{2.11}$$

Even after max approximation, the computational complexity is still exponential for calculating LLR. For computing the maximum in the numerator and denominator, two exhaustive searches are to be carried out over two non overlapping sets. Each of the set is with cardinality $2^{\sum_{k=1}^{4} m_k - 1}$ where m_k indicates the modulation order of k^{th} UE. Moreover, both of the sets are to be computed for every sample. For a simple case where all UEs are QPSK modulation, cardinality of both the sets are 128. On top of these computation processes, it is to be repeated for all the bits of all UEs. One way to reduce the computational complexity is to reuse the set X which was calculated for the first bit and subsequently reduce the number of search for maxima computation. The whole process is comprised of three steps defined as creation of superset, partitioning the set into two non overlapping sets and Identification of maxima from two sets.

Creation of Superset

For a given y_i and channel realisation $\underline{\mathbf{H_i}}$, super set X consists of all the terms in the numerator and denominator of (2.9). Creating the super set includes computing these terms and storing them in the memory appropriately. For all symbols of all the UEs ,$H_{i,k}x$ are found initially. Using the combinations of $H_{i,k}x$ and yi, all the terms in X will be evaluated. This result will be saved in the memory, where memory locations depends on which combinations of the symbols are used for evaluating the individual terms. An illustration is given in Fig. 2.4 where it is assumed that all the UEs are using QPSK for transmission.

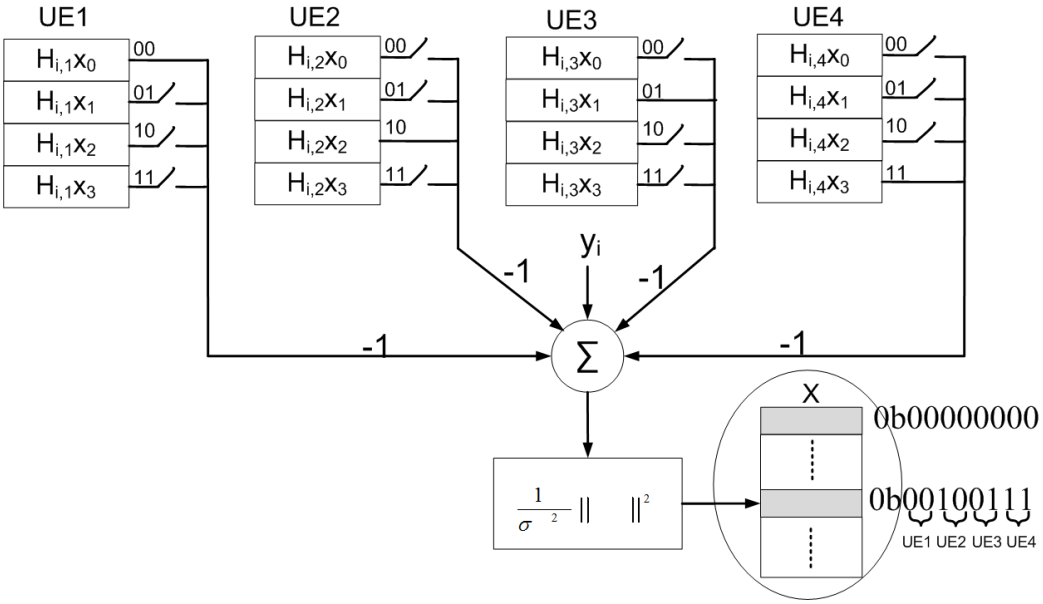

Fig. 2.4 Superset creation : Generation of data for the address location 0x27

Partition the set

For computing LLR of λ^{th} bit of k^{th} UE, we define two sets $X_{0,k,\lambda}$ and $X_{1,k,\lambda}$ corresponds to numerator and denominator. The sets are created as follows

$$\begin{aligned} X_{0,k,\lambda} &= \{x \in X |\ Addr(x)\ \&\ b(k,\lambda) \neq 0\} \\ X_{1,k,\lambda} &= \{x \in X |\ Addr(x)\ \&\ b(k,\lambda) = 0\} \end{aligned} \tag{2.12}$$

where $Addr(x)$ denotes the address of x, $b(k,\lambda)$ is a bit stream with length is equal to number of bits in the address representation of x and only single one is filled at position corresponding to λ^{th} bit of k^{th} UE.

Computation of Maximum in two sets

The sets $X_{0,k,\lambda}$ and $X_{1,k,\lambda}$ defined in previous subsection is having the following properties.

$$X_{0,k,\lambda} \cup X_{1,k,\lambda} = X \quad X_{0,k,\lambda} \cap X_{1,k,\lambda} = \Phi \tag{2.13}$$

$$max\{X\} = max\{max\{X_{0,k,\lambda}\}, max\{X_{1,k,\lambda}\}\} \tag{2.14}$$

While computing the LLR for first time, maximum will be found from both the sets by using exhaustive search algorithms. Maximum of X, $max\{X\}$, is

found by using (2.14). For all subsequent LLR computations, only one exhaustive search will be carried out because $max\{X\} \in \{max\{X_{0,k,\lambda}\}, max\{X_{1,k,\lambda}\}\}$. In $addr(max\{X\})$, if λ^{th} of k^{th} UE bit position is one, then $max\{X_{0,k,\lambda}\}$ is same as $max\{X\}$ otherwise $max\{X\}$ is the maximum of the set $X_{1,k,\lambda}$.
LLR is computed as follows.

$$LLR\_UE_{k,\lambda} = max\{X_{0,k,\lambda}\} - max\{X_{1,k,\lambda}\} \tag{2.15}$$

2.2.2 LLR Quantization

Having discussed an efficient computational technique for multiple LLRs, next interesting aspect is on how to quantize the LLR. Many papers on HARQ described about the non uniform quantization technique where the constraint is kept on either Mean Square Error (MSE) reduction [17] or maximizing Mutual Information (MI) [18]. Similar to these techniques, we have worked out a scheme to reduce the final bit error rate because of LLR quantization. We also consider the objective of reduction in number of bits per LLR. At higher and lower SNR, reducing the number of bits in LLR representation and thus increasing the quantization error does not result in much variation in BLER performance. In our case, we considered non uniform quantization using clustering technique and performance is compared with uniform quantization technique. Moreover number of bits per LLR are adaptively varied to get the best possible reduction in the bandwidth requirement.

Each LLR has sign and magnitude component where magnitude indicates the quality of LLR. By assuming that the adjacent bits are independent and randomly selected, sign of LLR of one bit does not provide any information about other bits. Hence, it is necessary to send the sign component of LLR for all the bits of UE. Magnitude component depends on noise properties, channel realisation and interference characteristic. For a block fading scenario, under the assumption of gaussian noise, absolute value of the LLR will be a mixture of gaussian. Clustering algorithm explores this property where each gaussian will be divided into single or multiple cluster and sends the cluster mean. In 1D clustering, all the LLRs in the block is treated independently while performing the quantization. In 2D

clustering, a new vector is generated by pairing adjacent bits [19] so that all the elements in the vector is of size two. The pairing depends on the modulation order and the PDF of the LLR for each bit. For QPSK modulation, since the modulation order is two, only one combination is possible. For 16QAM, each symbol has four bits and multiple combinations are possible. Pairing will be done based on the bits whose LLR PDFs are similar characteristic. The Fig.2.5 provide LLR PDF conditioned on transmitted bit equal to one, where we can see that 0^{th} bit and 2^{nd} bits has similar PDF and 1^{th} bit and 3^{rd} bits has similar PDF. Hence, bit-0 and bit-2 are paired and bit-1 and bit-2 are paired. The PDFs are obtained by carring out the simulation over AWGN channel for various SNRs and gray coding is used for symbol mapper as mentioned in [20]. It is assumed that the scenario is interference free.

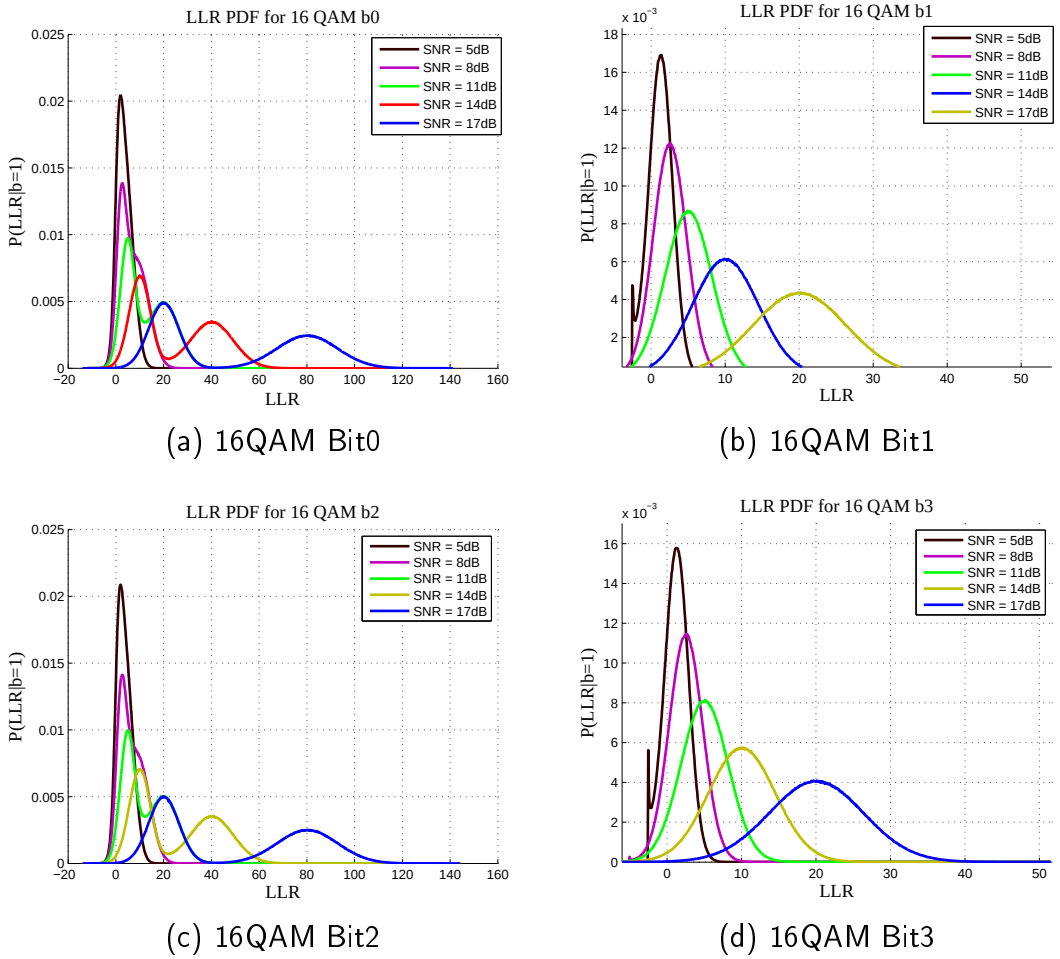

(a) 16QAM Bit0 (b) 16QAM Bit1

(c) 16QAM Bit2 (d) 16QAM Bit3

Fig. 2.5 LLR PDF for various bits of 16QAM

The algorithm for the adaptive clustering based quantization is given below.

- Initialise the number of iterations, number of clusters, N and cluster mean. Cluster mean for the first iteration is by randomly picking N elements from the set.
- Associate each element in the set with one of the cluster by using minimum Euclidean distance criteria.
- Recompute the cluster mean for all clusters.
- Compare each cluster mean with threshold on both dimension. In case of 1D clustering, threshold comparison is done only in one dimension.
- Repeat for multiple iteration.
- Merge the cluster with the adjacent cluster if the cluster mean is above the threshold. Adjacent cluster is in direction where threshold comparison is done.

At the end of this algorithm number of clusters, cluster mean and associated elements for each cluster will be provided as an output. These information along with sign component of LLR will be provided from eNodeB to serving node. Fig. 2.6 illustrates 2D clustering where clustering started with 8 clusters and ended with 4 clusters.

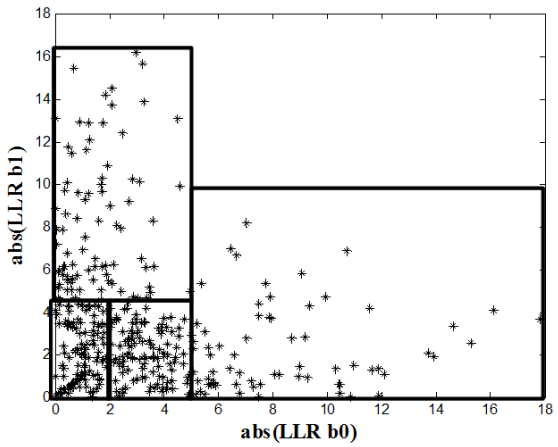

Fig. 2.6 2D Clustering with eight initial number of cluster

The mentioned algorithm will be done on request from other eNodeBs. Otherwise raw LLR will be stored in the buffer and flushed out later if no eNodeB request happens for LLR.

2.2.3 LLR Combining

LLR combining will be done based on the quality of LLR from all the eNodeBs in a cell. Combining is done as follows.

$$LLR_{sum} = \sum_{i=1}^{4} k_i * LLR_i \tag{2.16}$$

Where LLR_i indicates LLR from i^{th} eNodeB and $k_i \in \{0, 1\}$ depends on the quality of LLR_i. Quality will be decided based on number of bits and cluster centre from different eNodeB.

2.3 Simulation Result

In simulation, we consider a total of 19 cells and each cell is equipped with 4 operators eNodeBs. ISD of 1000m is taken for simulation. 20 UE per operator is randomly dropped in every cell. For cells other than centre cell, one UE per operator is selected randomly. For centre cell, UE selection depends on the simulation scenario like cell centre, cell edge etc. Simulation parameters are given in Table 2.1 Fig. 3.6 shows LLR pdf for various SNRs. It is observed from the figure that the

Table 2.1 Simulation parameter for uplink LLR combining

Sl No	Attribute	Value
1	Path loss exponent	2.5
2	Shadowing loss	8dB
3	Frequency Reuse	3
4	Receiver noise figure	6dB
5	Receiver bandwidth	10MHz
6	FEC Coding	Turbo code
7	Code rate	1/3
8	Block Length	256
9	CRC length	16
10	Generator polynomial	$x^{15} + x^{12} + x^5 + 1$

PDF can be modelled as a mixture of Gaussian. The number of individual Gaussian in the mixture depends on the channel realisation from UEs to eNodeB and the modulation order of UEs belonging to all the operators. This result motivates us to do non uniform quantization with variable number of bits for representing

LLR. Another observation from LLR PDF is that, PDF is symmetric with respect to origin as expected (Assuming prior probability for transmitting one and zero is equal).

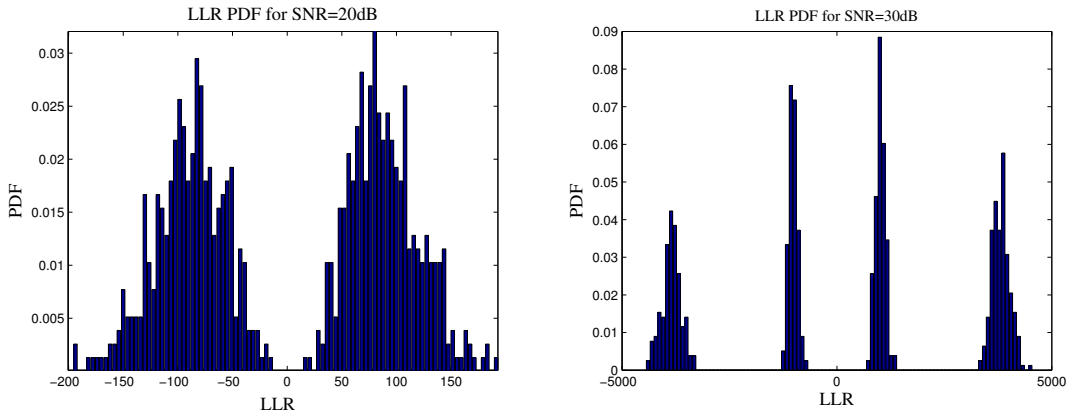

(a) SNR=20dB (b) SNR=30dB

Fig. 2.7 LLR PDF for various SNRs

The performance of the proposed technique depends on the number of modelled interferers in the LLR computation block. Fig. 2.8 demonstrates the performance of the LLR combiner for a reuse-1 cellular network where the number of modelled interferer is varied from zero to four. It is evident from the figure that at low SNR($<$15dB) performance is almost similar. Subsequently, we can see that the flooring of the BLER curve if the number of modelled interferer is less in the joint LLR computation block. As expected, if interferes are not modelled, the corresponding BLER curve floored first. Subsequently, the curve corresponds number of modelled interferer of one and two floored respectively. If the number of modelled interferers are three or more, the flooring of the curve is not observed. Important to note that, the number of operators in the single cell is four and hence the number of main contributors for the interference is three. The result, in general varies where performance with four modelled interferer may be much better if the fourth interferer is strong.(The result is only for a single realisation of the UE drop and fourth interferer became a weak interferer in this case)

The above work has been extended to reuse-3 cellular network. Fig.2.9 demonstrates the performance of reuse-3 cellular system. Compared to reuse-1 system, performance is seen to be better because of less number of unmodelled interferer

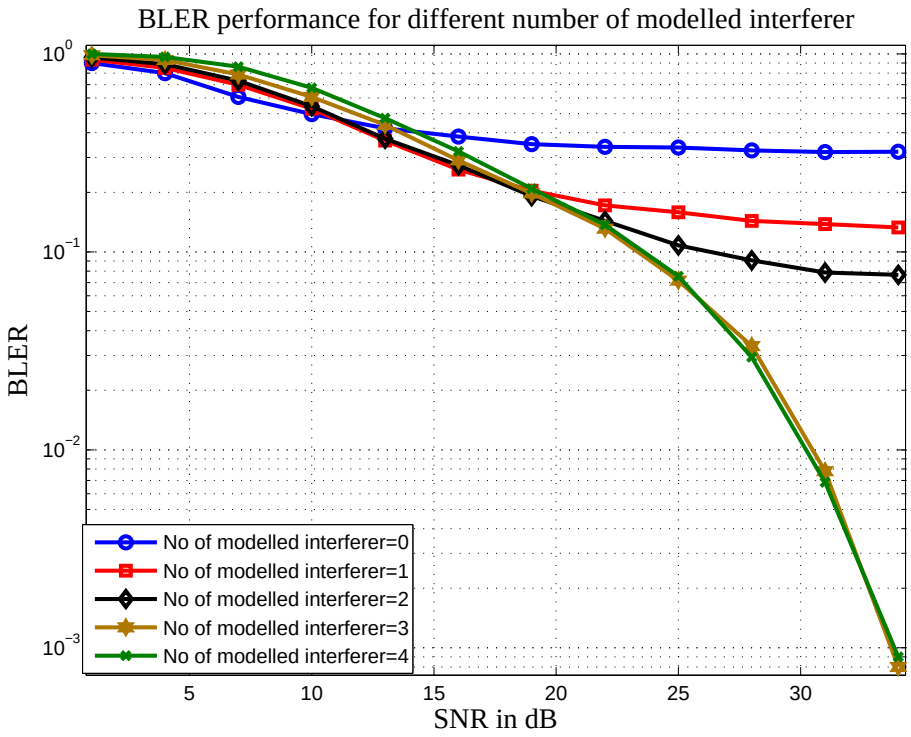

Fig. 2.8 BLER performance for different number of modelled interferer

and thus, better SINR in this system. From these two results, we can conclude that if the system is with fractional frequency reuse, performance should be between reuse-1 and reuse-3.

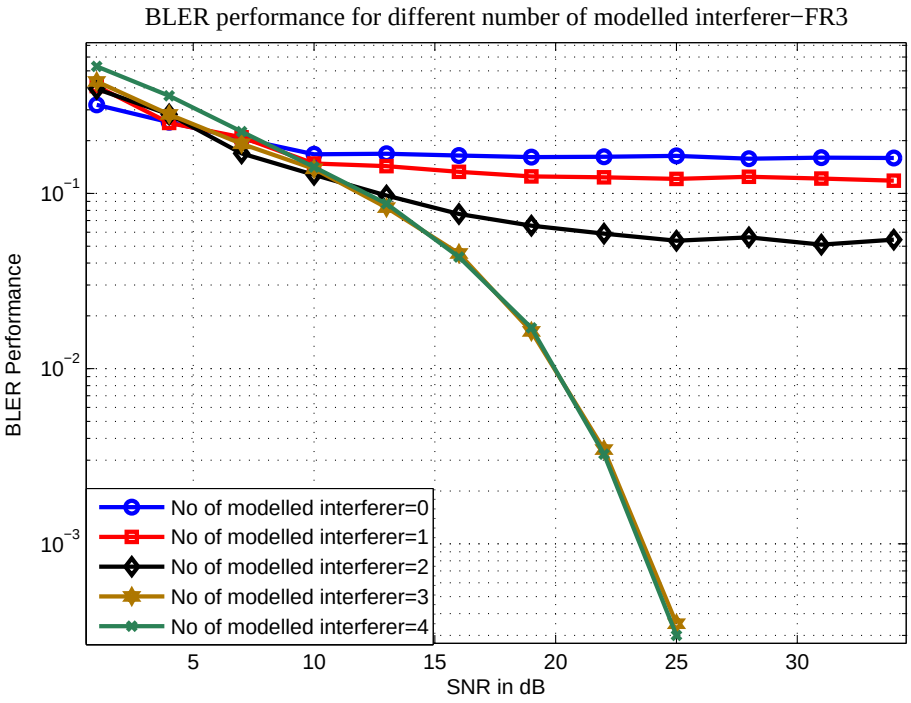

Fig. 2.9 BLER performance for different number of modelled interferer in FR3

Fig. 2.10 demonstrates the performance enhancement by using LLR combining with infinite precision representation of LLR and uniform quantization of LLR. The BLER result shows noticeable performance improvement by LLR combining. For e.g. at BLER of 1×10^{-4}, ideal LLR combiner gives a performance improvement of 12dB. The result in general varies with the position of UE and eNodeB. For uniform quantization, we have varied the number of bits per LLR from 2 to 6. In simulation, it is assumed that LLR combining is happening at serving eNodeB. Hence LLR corresponds to the serving eNodeB is not quantized while combining. The result also shows that 3 bit quantization will be sufficient to achieve the performance within 0.6dB. Hence, subsequent analysis is restricted to number of bits less than or equal to three.

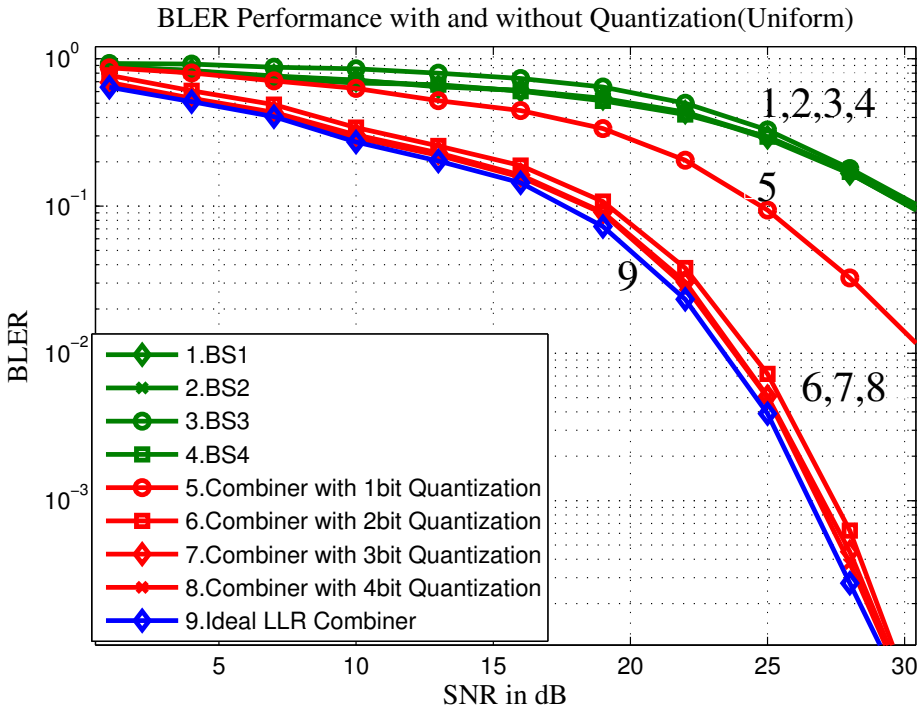

Fig. 2.10 BLER performance with LLR Combiner for uniform quantisation of LLR and without quantization(Ideal).

Fig. 2.11 demonstrates the performance of various non uniform quantization techniques. The performances is analysed for 1D clustering and 2D clustering based quantization. Result shows that the performance of clustering based quantization gives similar performance of uniform quantization at reduced number of bits per LLR. Moreover, performance of 2D based clustering technique is better than 1D based clustering technique.

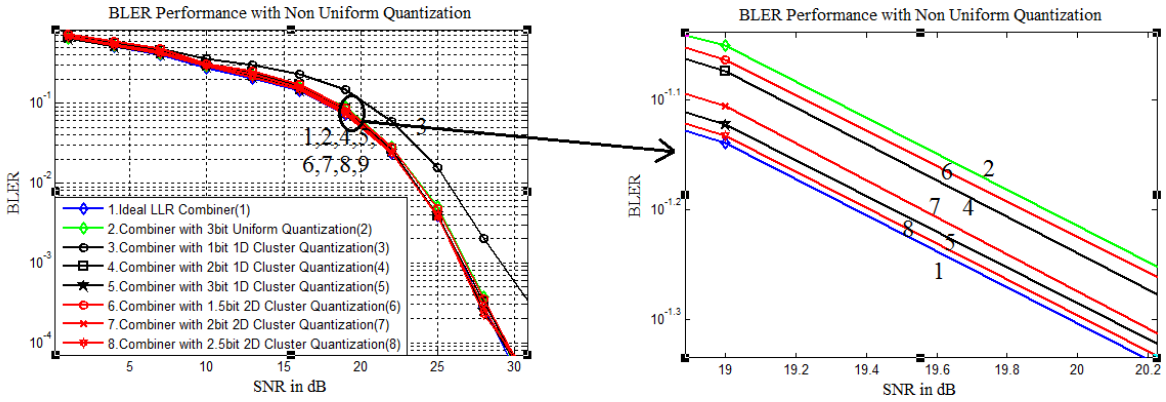

Fig. 2.11 BLER performance for non uniform quantization of LLR

Fig. 2.12 shows the performance of proposed technique for two networks namely network 1 and network 2. Network 1 is with OCR of 200m and network 2 is with OCR of 300m. In network 2, UEs belonging to eNodeB1 are dropped in such a way that they are far from eNodeB1 and close to one of the other eNodeBs. One of the inferences from the result is that the performance of adaptive clustering

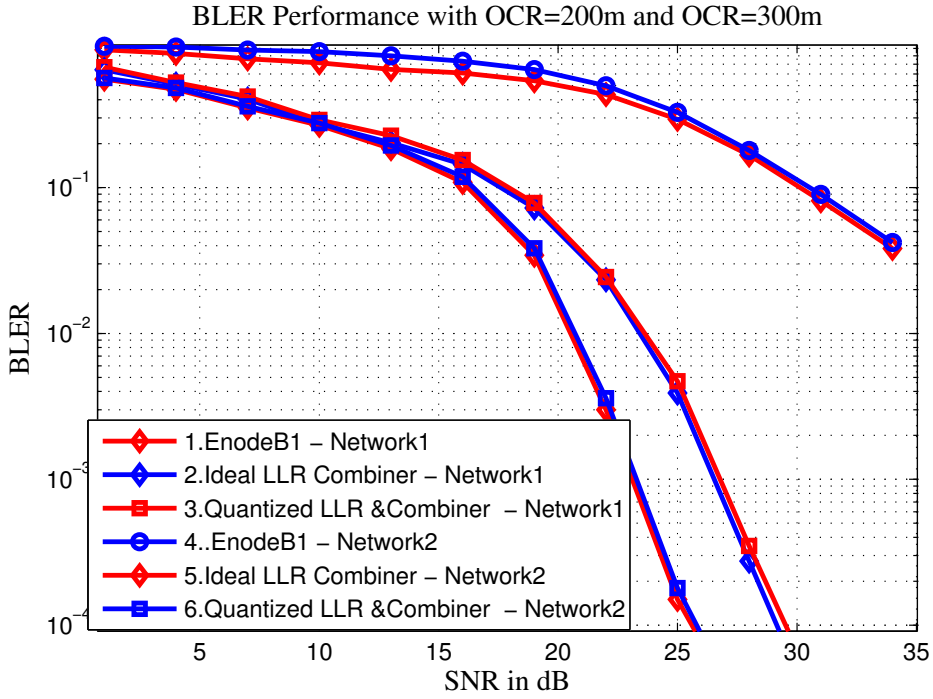

Fig. 2.12 BLER performance for the proposed method for network 1 and network 2

based non uniform quantization technique is within 0.3dB as compared to ideal LLR combiner. Moreover, it is evident from the figure that performance of UE at eNodeB1 is same for both networks. But the combined performance at serving node for UE1 is better in network 2. This is due to the fact that in network2, UE

is near to one of the operator eNodeB other than eNodeB1 and LLR quality is very good at that eNodeB and hence better combining gain is achieved. In general performance will be improved by LLR combining but the simulation result demonstrates for a combination of UE and eNodeB position, typically varied in a practical cellular network.

Fig. 2.13 shows the effective number of bits per LLR in the adaptive 2D clustering method for network 1 and network 2. The results varies with eNodeB position, UE position and channel realisation. It is evident from the figure that if the eNodeB sees a good channel from UE, even though the SNR at the serving station is not good, number of bits per LLR will be less. Moreover, at medium and higher SNR regime, optimal performance is achieved with less than 2bits per LLR.

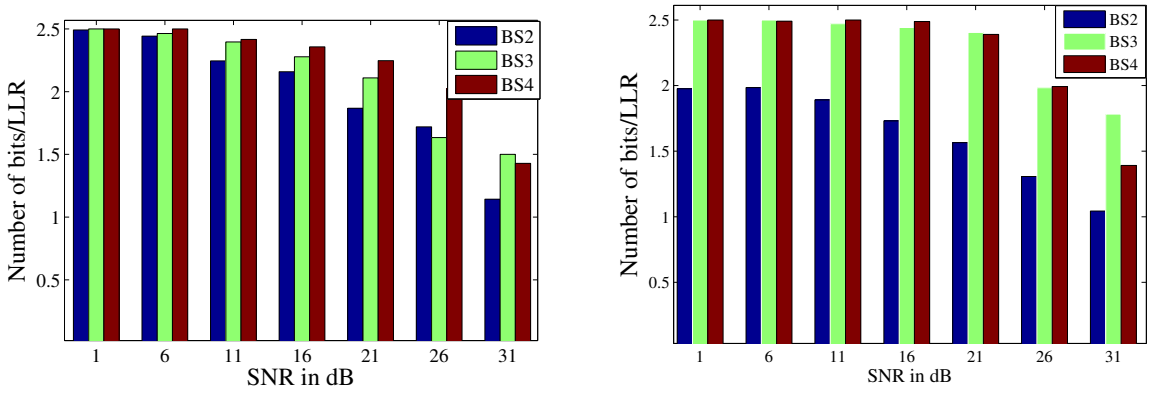

(a) OCR=200m (b) OCR=300m

Fig. 2.13 Number of bits/LLR for various SNR

CHAPTER 3

UPLINK ROBUST LLR

The LLR combing technique in a shared spectrum operation showed a huge improvement in the performance of the cellular network. Another important aspect of the work is to model the interference while computing the joint LLRs for multiple UEs at eNodeB. In a cellular network, transmission scenario and hence the interference profile varies with frequency management/reuse schemes and carrier aggregation. For example, consider the case where the cellular network is having carrier aggregation by use of Industrial, Scientific, and Medical (ISM) band and non-ISM band of frequencies as shown in Fig. 3.1. In this scenario, it is expected

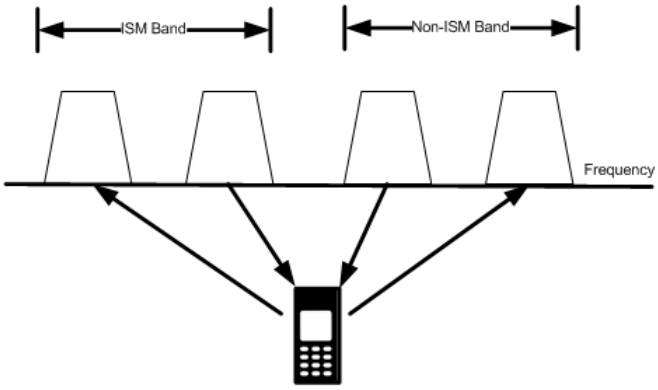

Fig. 3.1 Carrier Aggregation by using ISM and Non-ISM Band of frequencies

that one set of contiguous resources are orthogonal resources (ICI free) for the operator as compared to remaining set of resources. In a shared spectrum operation, it is expected to have orthogonal resources to individual operators along with the shared part of the spectrum. Hence, there can be scenarios similar to aforementioned carrier aggregation technique by using orthogonal and non-orthogonal resources together(especially when the network is lightly loaded). Another case is that, due to resource block allocation and different loads across the network, interference from each eNodeB affects randomly across a small fraction of the frequency spectrum. However, the affected resource block may vary from one interferer to another. In our system model, we capture these changes in the interference as multiple scenarios.

3.1 System Model

We consider a 19 cell model for the analysis of the proposed technique and performance is monitored at the centre cell and two adjacent cells, denoted here as coordinating cells. A detailed sketch is given in Fig. 3.2, where three UEs are connected simultaneously to three eNodeBs. The cell centres are separated by a constant distance, denoted here as Inter Site Distance (ISD). It is assumed that

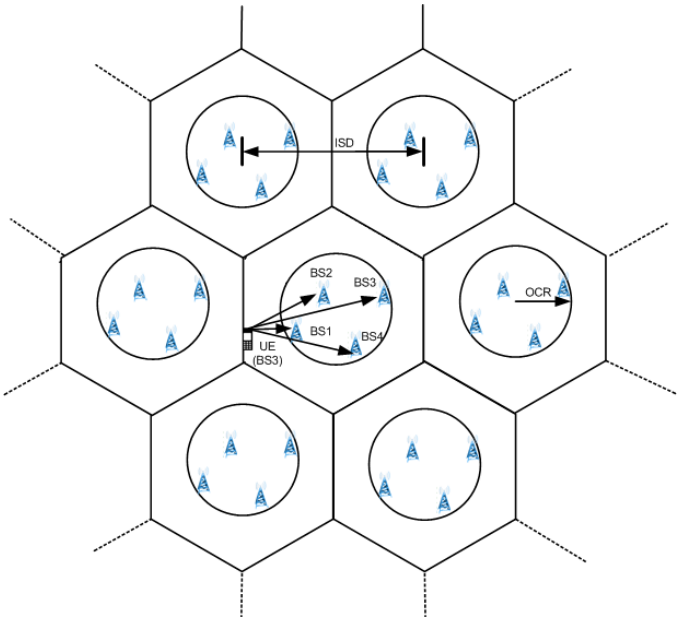

Fig. 3.2 Cellular network with 4 operator per cell

the UEs from coordinating cells are simultaneously transmitting in the same subcarriers and other UEs transmission, ICI, may partially occupy these subcarriers. The number of subcarriers which are being affected due to ICI depends on the ICI mitigation plan and transmission scenario. In our model, we capture two scenarios denoted as Scenario 1 and Scenario 2. In Scenario 1, it is assumed that only fraction of subcarriers are affected due to interference and the remaining are interference free subcarriers. In Scenario 2, each interferer affects a fraction of the subcarriers and the affected subcarriers due to each interferer varies randomly.

The received signal at each eNodeB will be a combination of signals from UE belonging to the same cell, UEs belonging to other operators in the same cells and UEs from all other cells. The received signal at the n^{th} eNodeB for any i^{th}

subcarrier can be represented as follows.

$$y_n(i) = H_{1,nn}(i)x_{1,n}(i) + \underbrace{\sum_{\substack{m\in I \\ m\neq n}} H_{1,mn}(i)x_{1,m}(i)}_{\text{Modeled Interferer}} + \underbrace{\phi(i)\sum_{k=2}^{M}\sum_{m\in I}\psi_k H_{k,mn}(i)x_{k,m}(i)}_{\text{Unmodeled Interferer}} + n_n(i) \tag{3.1}$$

$$y_n(i) = H_{1,nn}(i)x_{1,n}(i) + \underbrace{\sum_{\substack{m\in I \\ m\neq n}} H_{1,mn}(i)x_{1,m}(i)}_{\text{Modeled Interferer}} + \underbrace{\sum_{k=2}^{M}\sum_{m\in I}\phi_k(i)\psi_k H_{k,mn}(i)x_{k,m}(i)}_{\text{Unmodeled Interferer}} + n_n(i) \tag{3.2}$$

where $n \in \{1,2,3,4\}$, $I \in \{1,2,3,4\}$, M denotes the number of cells considered, and $H_{k,mn} = \sqrt{\alpha_{k,mn}\beta_{k,mn}\gamma_{k,n}}h_{k,mn}$ denotes the instantaneous channel denote the instantaneous channel from UE of the m^{th} operator from k^{th} cell to n^{th} eNodeB. Here, $\alpha_{k,mn}$ and $\beta_{k,mn}$ represent the path loss and shadowing fading from UE of m^{th} operator from k^{th} cell to n^{th} eNodeB respectively. Also $\gamma_{k,n}$ indicates the transmitter power of UE belonging to the n^{th} eNodeB of k^{th} cell, which is being adjusted to get a specified Signal to Interference Ratio (SIR) and details are given in the next paragraph. The element $h_{k,mn}$ is an independent and identically distributed complex Gaussian random variable with zero mean and unit variance. In (3.1) and (3.2), $x_{k,m}(i)$'s are symbols from unit modulus constellation. Also, $\psi_k \in \{0,1\}$ where its value depends on frequency management scheme. For example, ψ_k is one for every k in frequency reuse one. Here, $E(\psi_k) = \psi$ where $E(.)$ denote the expectation operator. Also, $\phi_k(i) \in \{0,1\}$ is the contribution from the k^{th} interferer and it is modelled as Bernoulli distribution with $p = \epsilon$, thus $E(\phi_k) = \epsilon$. $\phi(i)$ is the i^{th} element of the vector $[\underline{\mathbf{0}}^{\mathbf{T}} \;\; \underline{\mathbf{1}}^{\mathbf{T}}]^{\mathbf{T}}$ where cardinality of $\underline{\mathbf{0}}$ and $\underline{\mathbf{1}}$ are $\epsilon \times N$ and $(1-\epsilon) \times N$ respectively. Here, N denotes the block length of the frame. $n_n(i)$ denotes the additive white complex gaussian noise with zero mean and variance σ^2. Noise variance in dBm is obtained as follows

$$\sigma^2 = -174 + 10log10(BW) + NF \tag{3.3}$$

where BW indicates the receiver bandwidth in Hz and NF indicates the noise figure in dB.

The transmit power of each interferer depends on the specified SIR at the centre cell. SIR is given as

$$SIR = \frac{E(S)}{E(\sum_{k=2}^{M} \sum_{m \in I} \phi_{k,m} \psi_k P_{k,m})} \tag{3.4}$$

where S denotes the signal power, and $P_{k,m}$ denotes interference power from m^{th} interferer from k^{th}. We can compute the E(S) from required SNR and noise power. Subsequently, expected value of the total interference power in the denominator, denoted as $E(P_{SUM})$, will be computed from SIR and $E(S)$. Each interferer power is computed as follows.

$$\begin{aligned}
E(P_{SUM}) &= E(\sum_{k=2}^{M} \sum_{m \in I} \phi_{k,m} \psi_k P_{k,m}) && (3.5)\\
&= \sum_{k=2}^{M} \sum_{m \in I} E(\phi_{k,m} \psi_k P_{k,m}) && (3.6)\\
&= \sum_{k=2}^{M} \sum_{m \in I} E(\phi_{k,m)E(\psi_k)E(P_{k,m})} && (3.7)\\
&= \epsilon\psi \sum_{k=2}^{M} \sum_{m \in I} E(P_{k,m}) && (3.8)
\end{aligned}$$

Linearity of expectation operation is applied in (3.6) and independence of the random variable is applied in (3.7) to get the result in (3.8). With out loss of generality, it is assumed that $E(P_{2,m}) = E(P_{3,m}) = \cdots = E(P_{M,m}) \quad \forall m$ and hence the interference power from each UE is

$$E(P_i) = \frac{E(P_{SUM})}{|I|(M-1)\epsilon\psi} \quad \forall i \in \{4, 5, \cdots, M\} \tag{3.9}$$

where $|x|$ indicates the cardinality of the set x. From $E(P_{i,m})$ and path loss, $\gamma_{i,m}$ is computed.

In this current study, we have assumed accurate channel estimates from UE to three eNodeBs are available for processing. Also, we assume that the modulation

order of all UEs in the cooperating cells are known to the eNodeBs for joint processing. The transmitter and receiver block for the UE is same as used in in chapter 2. It is also assumed that eNodeBs are connected to one another via high speed link for exchanging the information.

3.2 LLR Generation Model, Robust LLR computation and LLR combining

The section describes the LLR generation models used for Robust LLR computation, Robust LLR computation of multiple UEs at eNodeBs and Robust LLR combining from multiple eNodeBs at serving node.

3.2.1 LLR Generation Model

Interferences from other cells are treated as impulsive noise while computing the LLR. Several models have been proposed for characterising impulsive noise. In our case, we have considered ϵ Gaussian-Gaussian mixture model, ϵ Gaussian-Laplacian mixture model, and ϵ Gaussian-Cauchy mixture and the LLRs are CG LLR, CL LLR, and CC LLR respectively. The PDFs are
ϵ Gaussian-Gaussian mixture:

$$f(x) = \frac{1-\epsilon}{\pi\sigma^2} exp(\frac{-x^2}{\sigma^2}) + \frac{\epsilon}{\pi\sigma_{nb}^2} exp(\frac{-x^2}{\sigma_{nb}^2}) \tag{3.10}$$

ϵ Gaussian-Laplacian mixture:

$$f(x) = \frac{1-\epsilon}{\pi\sigma^2} exp(\frac{-x^2}{\sigma^2}) + \frac{\epsilon}{\pi\sigma_{nb}^2} exp(\frac{-2|x|}{\sigma_{nb}}) \tag{3.11}$$

ϵ Gaussian-Cauchy mixture:

$$f(x) = \frac{1-\epsilon}{\pi\sigma^2} exp(\frac{-x^2}{\sigma^2}) + \frac{\epsilon\gamma}{\pi(x^2+\gamma^2)} \tag{3.12}$$

where σ_{nb} is the variance estimate of the unknown interference term in (3.1) and (3.1), and γ is adjusted to get the Geometric-Signal-to-Noise-Ratio (GSNR) of Cauchy PDF same for Gaussian PDF, as mentioned in [26] .

3.2.2 Robust LLR Computation

Since the received signal consists of signals from multiple UEs, LLR for multiple UEs can be calculated at the eNodeB. For any time instant i, given the received signal y_i, and channel from UEs to eNodeB $\underline{\mathbf{H_i}}$, LLR for λ^{th} bit of k^{th} UE is defined as

$$LLR\_UE_{k,\lambda} = \ln \frac{Pr\{b_\lambda = 1 | y_i, \underline{\mathbf{H_i}}\}}{Pr\{b_\lambda = 0 | y_i, \underline{\mathbf{H_i}}\}} \tag{3.13}$$

where $k \in \{1, 2, 3, 4\}$, $\lambda \in \{1, 2, 3, \cdots, m_k\}$, and m_k indicates the modulation order of the k^{th} UE. By using Bayes rule, (3.13) is expanded as follows

$$LLR\_UE_{k,\lambda} = \ln \frac{Pr\{y_i | b_\lambda = 1, \underline{\mathbf{H_i}}\} Pr\{b_\lambda = 1\}}{Pr\{y_i | b_\lambda = 0, \underline{\mathbf{H_i}}\} Pr\{b_\lambda = 0\}} \tag{3.14}$$

Without loss of generality, it is assumed that prior probabilities for transmitting one and zero is the same. Then, (3.14) can be written as

$$LLR\_UE_{k,\lambda} = \ln \frac{Pr\{y_i | b_\lambda = 1, \underline{\mathbf{H_i}}\}}{Pr\{y_i | b_\lambda = 0, \underline{\mathbf{H_i}}\}} \tag{3.15}$$

Let all the symbols for k^{th} UE belong to set X. Defining two non-overlapping sets X_0 and X_1 as follows

$$X_0 = \{x \in X | b_\lambda = 0\} \quad X_1 = \{x \in X | b_\lambda = 1\} \tag{3.16}$$

We can compute (3.15) as

$$LLR\_UE_{k,\lambda} = \ln \frac{\sum\limits_{x \in X_1} Pr\{y_i | x, \underline{\mathbf{H_i}}\}}{\sum\limits_{x \in X_0} Pr\{y_i | x, \underline{\mathbf{H_i}}\}} \tag{3.17}$$

Now by applying the conditional probability definition, LLR for λ^{th} bit of k^{th} UE

is given as

$$LLR\_UE_{k,\lambda} = ln\frac{a+b}{c+d} \tag{3.18}$$

where

$$a = \sum_{x\in X_1}\sum_{\underline{s}\in I}\frac{(1-\epsilon)}{\pi\sigma^2}\exp\{\frac{-1}{\sigma^2}\|y_i - H_{i,k}x - \sum_{\substack{m\in M\\ m\neq k}} H_{i,m}s_m\|^2\}$$

$$c = \sum_{x\in X_0}\sum_{\underline{s}\in I}\frac{(1-\epsilon)}{\pi\sigma^2}\exp\{\frac{-1}{\sigma^2}\|y_i - H_{i,k}x - \sum_{\substack{m\in M\\ m\neq k}} H_{i,m}s_m\|^2\}$$

For the ϵ Gaussian-Gaussian mixture:

$$b = \sum_{x\in X_1}\sum_{\underline{s}\in I}\frac{\epsilon}{\pi\sigma_{nb}^2}\exp\{\frac{-1}{\sigma_{nb}^2}\|y_i - H_{i,k}x - \sum_{\substack{m\in M\\ m\neq k}} H_{i,m}s_m\|^2\}$$

$$d = \sum_{x\in X_0}\sum_{\underline{s}\in I}\frac{\epsilon}{\pi\sigma_{nb}^2}\exp\{\frac{-1}{\sigma_{nb}^2}\|y_i - H_{i,k}x - \sum_{\substack{m\in M\\ m\neq k}} H_{i,m}s_m\|^2\}$$

For the ϵ Gaussian-Laplacian mixture:

$$b = \sum_{x\in X_1}\sum_{\underline{s}\in I}\frac{\epsilon}{\sigma_{nb}^2}\exp\{-\sqrt{\frac{1}{\sigma_{nb}^2}}|y_i - H_{i,k}x - \sum_{\substack{m\in M\\ m\neq k}} H_{i,m}s_m|\}$$

$$d = \sum_{x\in X_0}\sum_{\underline{s}\in I}\frac{\epsilon}{\sigma_{nb}^2}\exp\{-\sqrt{\frac{1}{\sigma_{nb}^2}}|y_i - H_{i,k}x - \sum_{\substack{m\in M\\ m\neq k}} H_{i,m}s_m|\}$$

For the ϵ Gaussian-Cauchy mixture:

$$b = \sum_{x\in X_1}\sum_{\underline{s}\in I}\frac{\epsilon\gamma}{2\pi((y_i - H_{i,k}x - \sum_{\substack{m\in M\\ m\neq k}} H_{i,m}s_m)^2+\gamma^2)^{1.5}}$$

$$d = \sum_{x\in X_0}\sum_{\underline{s}\in I}\frac{\epsilon\gamma}{2\pi((y_i - H_{i,k}x - \sum_{\substack{m\in M\\ m\neq k}} H_{i,m}s_m)^2+\gamma^2)^{1.5}}$$

where I denotes all possible symbol combination for known interferers and $M = \{1, 2, 3\}$.

Robust LLR computation in (3.18) involves computing exponential function of the form $y \times exp(-x)$. Depending on the value of x, direct evaluation of the exponential function in a hardware may result in underflow and hence LLR can be erratic. Since the numerator and denominator in (3.18) are Log Sum Exponential, in order to make the computation more efficient with less error, jacobian algorithm [16] is applied.

$$ln(exp(x_1) + \cdots + exp(x_n) = x^* + ln(exp(x_1 - x^*) + \cdots + exp(x_n - x^*)) \tag{3.19}$$

where

$$x^* = max(x_1, x_2, \cdots, x_n) \tag{3.20}$$

For applying the jacobian algorithm, exponential function of the form $y \times exp(-x)$ is modified as $exp(-x + ln(y))$. For example, a in (3.18) is written as
$a = \sum_{x \in X_1} \sum_{\underline{s} \in I} \exp\{\frac{-1}{\sigma^2} \| y_i - H_{i,k}x - \sum_{\substack{m \in M \\ m \neq k}} H_{i,m}s_m \|^2 + ln(\frac{(1-\epsilon)}{\pi\sigma^2})\}$
The other terms b,c,d in (3.18) is also follows in a similar manner.

3.2.3 LLR Combining

LLR combining is done as follows.

$$LLR_{sum} = \sum_{i=1}^{4} k_i LLR_i \tag{3.21}$$

where LLR_i indicates LLR from i^{th} eNodeB and $k_i \in \{0, 1\}$ depends on the quality of LLR. The combining is equivalent to selection gain combining as described in [27].

3.3 Simulation Results

For simulation, we consider a total of 19 cells with ISD of 1000m and eachcell is equipped with 4 operators. 20 UEs per operator is randomly dropped in every cell. For cells other than centre cells, one UE per operator is selected randomly. For centre cells, cell edge UEs are selected. The simulation parameters are given in Table 3.1.

Before considering the scenarios as mentioned in the system model, the performance of the Robust LLR based multiuser detection scheme is analysed by taking the interference term in (3.1) and (3.2) as the realisation of a complex Gaussian random variable. For this random variable, mean is set to zero and variance is set such that SIR of 3dB is obtained at the centre cell eNodeB. Here, simulation set up is similar to scenario 1 with $\epsilon = 0.3$. Fig. 3.3 demonstrates the performance enhancement by using Robust LLR technique for the mentioned simulation setup.

Table 3.1 Simulation parameter for Robust LLR

Sl No	Attribute	Value
1	Path loss exponent	2.5
2	Shadowing loss	8dB
3	Receiver noise figure	6dB
4	Receiver bandwidth	10MHz
5	FEC Coding	Turbo code
6	Code rate	1/3
7	Block Length	256
8	CRC length	16
9	Generator polynomial	$x^{15} + x^{12} + x^5 + 1$

The BLER curve shows a noticeable performance increment by using Robust LLR technique as compared to Gaussian LLR. Moreover, huge performance improvement is shown in the BLER result after LLR combining. For example, at BLER of 10^{-2}, the performance improvement by CG LLR, CC LLR and CL LLR are around 15dB.

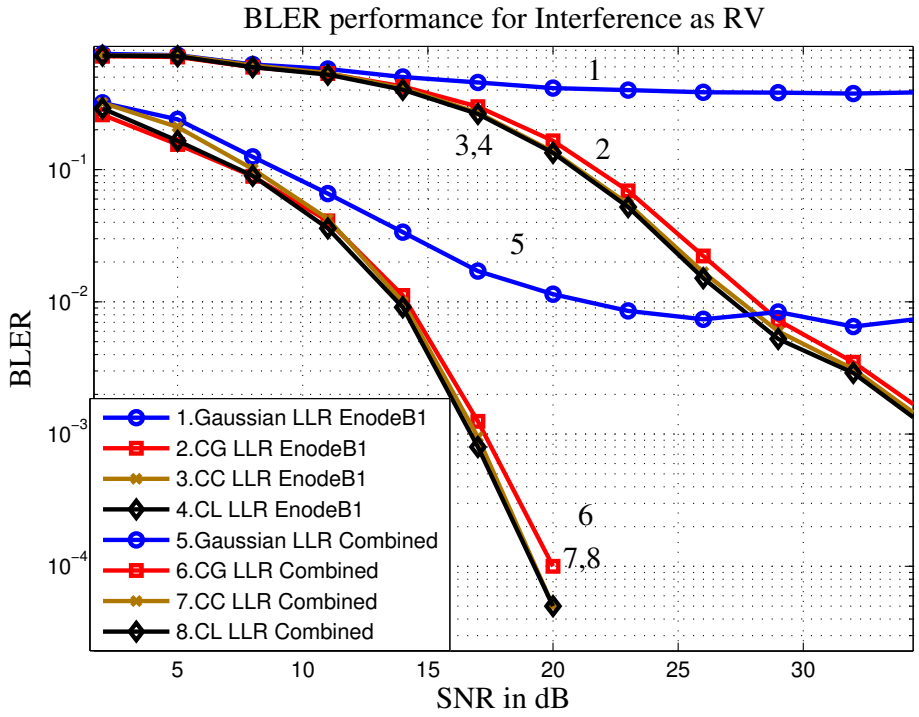

Fig. 3.3 BLER performance when interference term as the realisation of a Random Variable

Fig. 3.9 demonstrates the performance of the proposed scheme for scenario 1 with $\epsilon = 0.3$ and SIR of 3dB. Simulation is carried out for various LLR generation model with and without LLR combining. It is evident from the figure that Gaussian LLR based approach floors approximately from 18dB. The same is

true even after combining the Gaussian LLRs. The performance of CC LLR, CG LLR, and CL LLR at the eNodeB is much better than the Gaussian LLR. Robust LLR combining shows noticeable performance improvement in the single antenna CoMP system described. The BLER performance with all the three Robust LLR models are within 0.4dB. CL LLR outperforms the CC LLR and CG LLR. At BLER of 10^{-3}, the improvement of combined CL LLR is around 18dB as compared to BLER performance of CL-LLR based multiuser detector at eNodeB1. One important observation from the result is that, if SNR is above 22dB, Robust LLR without LLR combining itself is better than the performance of combined Gaussian LLR based approach.

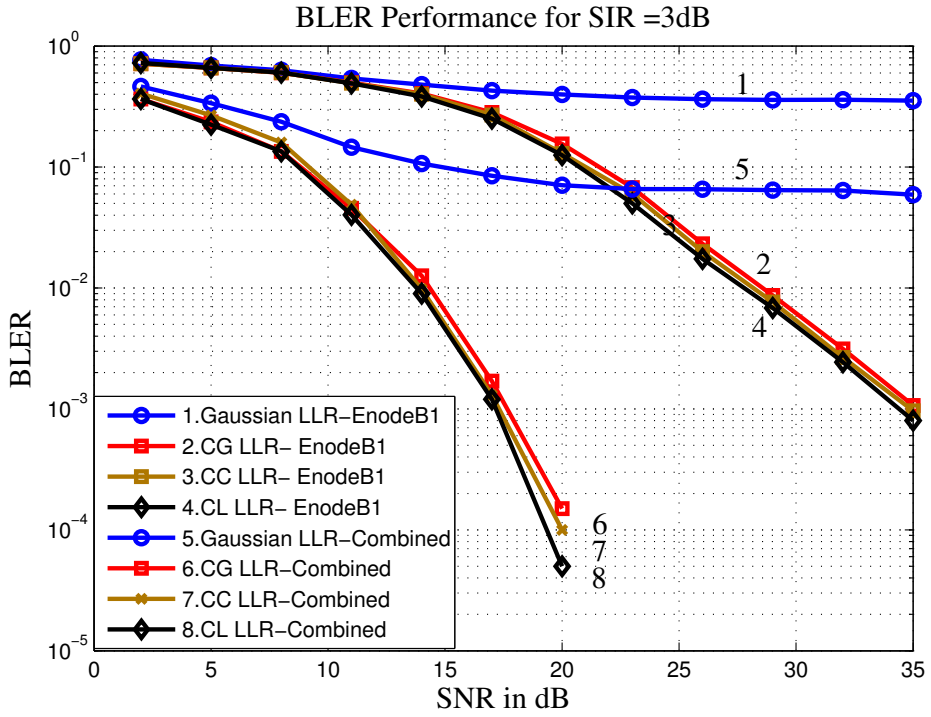

Fig. 3.4 BLER performance for scenario 1

Fig. 3.10 compares the performance of the proposed scheme in Scenario 2 for various LLR generation models with and without LLR combining. The ϵ is set to 0.3 and SIR of 3dB is used for simulation. Unlike in Scenario 1, most of the subcarriers are getting affected by interference in Scenario 2. The result also dictates the same by showing the poor performance in Scenario 2 as compared to Scenario 1. As compared to Scenario 1, at each eNodeB, performance gap between the Robust LLR and Gaussian LLR is negligible in Scenario 2. One important inference from the result is that, all mentioned LLRs including Robust LLRs based

technique floor at medium SNR onwards. Also, at higher SNR Gaussian LLR based method performed similar to CG LLR. Moreover, performance variation across Robust LLRs is noticeable in scenario 2. BLER performance of CG LLR is best among all the three models and performance of CC LLR is seen to be the worst.

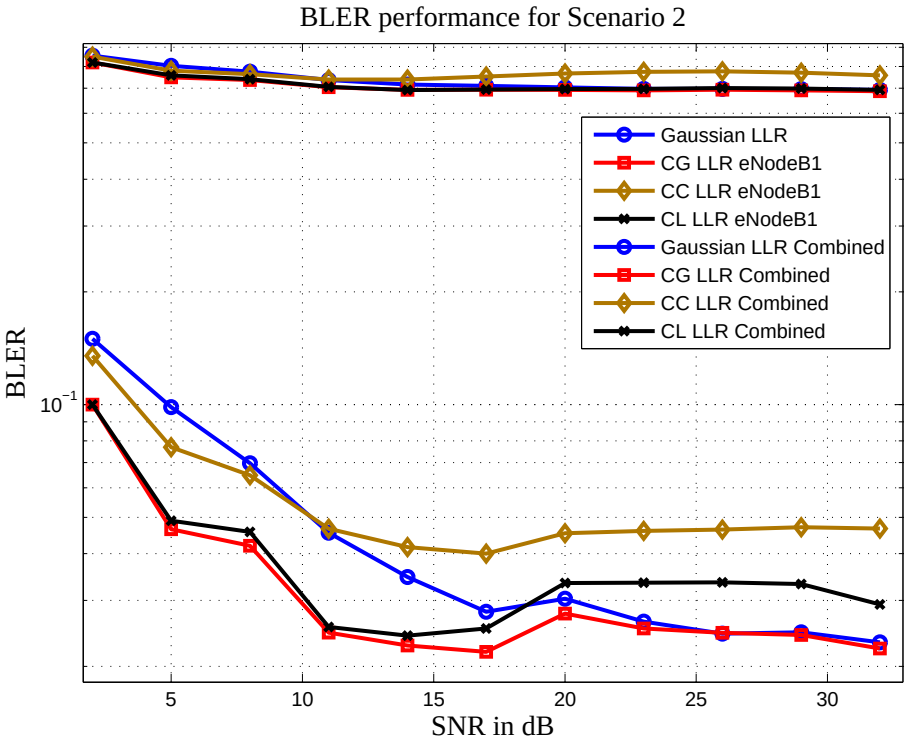

Fig. 3.5 BLER performance for scenario 2

Fig. 3.6 compares the performance of the proposed scheme in Scenario 1 for ϵ of 0.5 ,0.3, and 0.1 with SIR of 3dB. The results are only with LLR combining and ϵ in the LLR generation models are fixed to 0.3. It is evident from the figure that, Robust LLR based scheme outperforms the Gaussian LLR in all the three cases considered. Also, as expected, the Gaussian LLR performance is better when the less number of subcarriers are affected due to interferers. Another important observation from the figure is related to change in performance of various Robust LLRs as the ϵ goes from higher value to smaller value in the simulation scenario. For higher values of ϵ, CC LLR based approximation is seen to be performing similar as compared to CG LLR and CL LLR. For smaller values of ϵ, CG LLR is the best candidate and CC LLR performance is the worst. In both the cases, CL LLR is very close to the best candidate and the performance gap is within 0.2dB.

Whenever, ϵ in the simulation scenario matches with the ϵ in the LLR generation model, all the three Robust LLRs performed nearly equal.

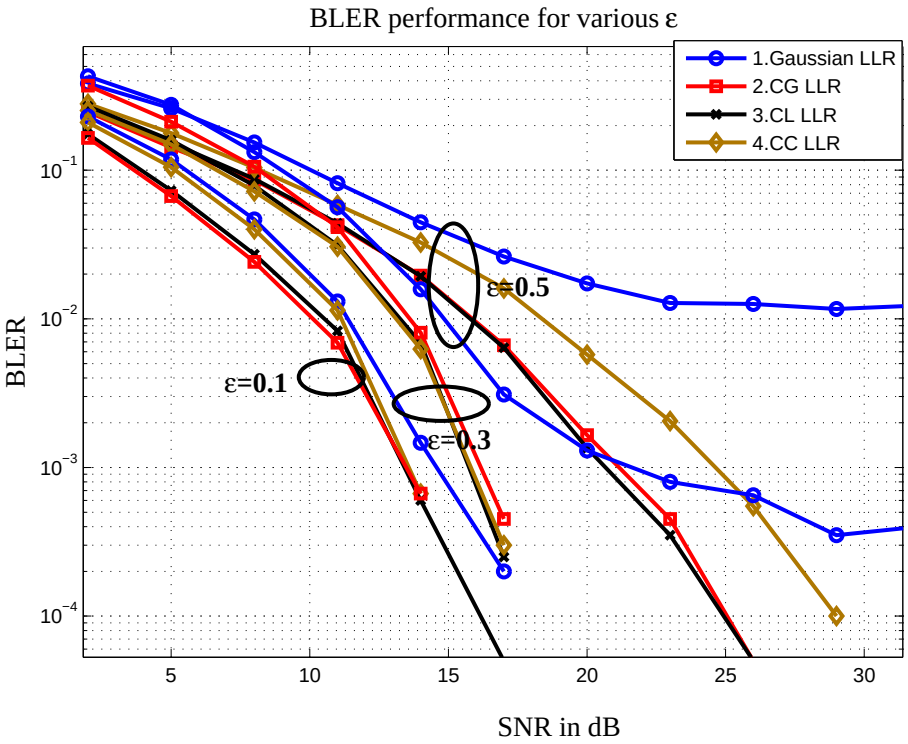

Fig. 3.6 BLER performance for scenario 1 for various ϵ in the transmission scenario and fixed ϵ in LLR generation model

Fig. 3.7 compares the performance of the proposed scheme in Scenario 2 for ϵ of 0.5 ,0.3, and 0.1 and LLR generation model is with ϵ of 0.37. The SIR is fixed as 3dB and once again simulation is carried out only with LLR combining. Irrespective of ϵ, it is observed that all the LLR generation models floor from some SNR onwards and that SNR depends on ϵ. If ϵ is small, more number of subcarriers are getting affected by interference and flooring happens from small value of SNR onwards. Another important inference from the figure is related to change in performance of various Robust LLRs as the ϵ goes from higher value to smaller value in the simulation scenario. Unlike in Scenario 1, CC LLR became the worst Robust LLR candidate in all three cases. Moreover, for higher value of SNR, the Gaussian LLR performance is better than CC LLR and CL LLR. The performance gap between CG LLR and CL LLR is seen to be negligible.

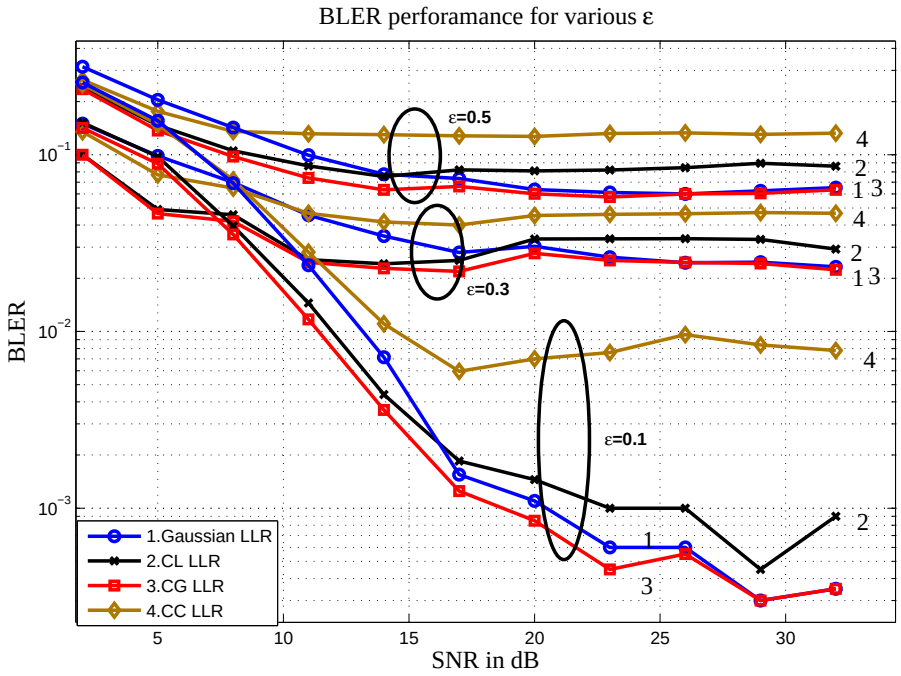

Fig. 3.7 BLER performance for scenario 2 for various ϵ in the transmission scenario and fixed ϵ in LLR generation model

3.4 Application of Robust LLR technique to SISO CoMP system

Co-operative communication is an efiňĄcient way of enhancing the quality of services in a wireless system [21] [22]. The application of cooperative communication in 4G Long Term Evolution (LTE) using 3GPP technology is Coordinated Multi-Point (CoMP) technique [23], used mainly for enhancing the performance of the cell edge user. The different techniques in CoMP are joint reception for the uplink and joint transmission and joint beam forming techniques for the downlink [2]. In joint reception, signal from a UE or UEs will be received by multiple eNodeBs and these signals are jointly processed to enhance the detection probability.

In 3GPP LTE, MIMO technique is used for better spectral efficiency. For single and multiple user case, SU-MIMO and MU-MIMO [24] is used respectively for enhancing the system performance. However, Inter Cell Interference (ICI) limits the upper bound performance of MIMO system in practical scenarios. In 3GPP LTE, CoMP is adopted for mitigating ICI [25]. These systems are known for their enhanced performance due to the multiple receive antennas, thus achieving the

diversity gain. Now, consider a scenario where the deployable cellular system is in UHF band, say centre frequency is 450MHz. In this system, the separation between the antenna elements are the order of 75cm. In case of small cell networks, this might not be a viable solution. In SISO links, there are many research papers addressing the issue of performance enhancement in uplink CoMP when a single users signal is orthogonally picked up by multiple base-stations (eNodeBs). In other words, for CoMP between N eNodeBs, interference management is done to ensure only one out of the N users transmits at a time on a given resource. In contrast to this technique, we propose a single antenna system which can handle multiple UEs associated to different eNodeBs at different cells. Here, we jointly decode the information pertaining to multiple UEs rather than treating the dominant signal from other UEs as interference. Decoded information will be shared to the mother eNodeB or centralised node for combining and therefore getting spatial diversity and receive diversity. The scheme is similar to robust LLR based uplink scheme described in the earlier sections.

3.4.1 SISO CoMP cellular network

We consider a 19 cell model for the analysis of the proposed technique and performance is monitored at the centre cell and two adjacent cells, denoted here as coordinating cells. A detailed sketch is given in Fig. 3.8, where three UEs are connected simultaneously to three eNodeBs. The scenarios are similar to earlier section except that each cell consist of only one eNodeB, corresponds to single operator case. Hence, (3.1) and (3.2) are modified as follows.

$$\text{Scenario 1: } y_n(i) = H_{n,n}(i)x_1(i) + \underbrace{\sum_{\substack{k=1 \\ k\neq n}}^{3} H_{k,n}(i)x_k(i)}_{\text{Known Interferer}} + \underbrace{\phi(i)\sum_{k=4}^{M}\psi_k H_{k,n}(i)x_k(i)}_{\text{Unknown Interferer}} + n_n(i) \tag{3.22}$$

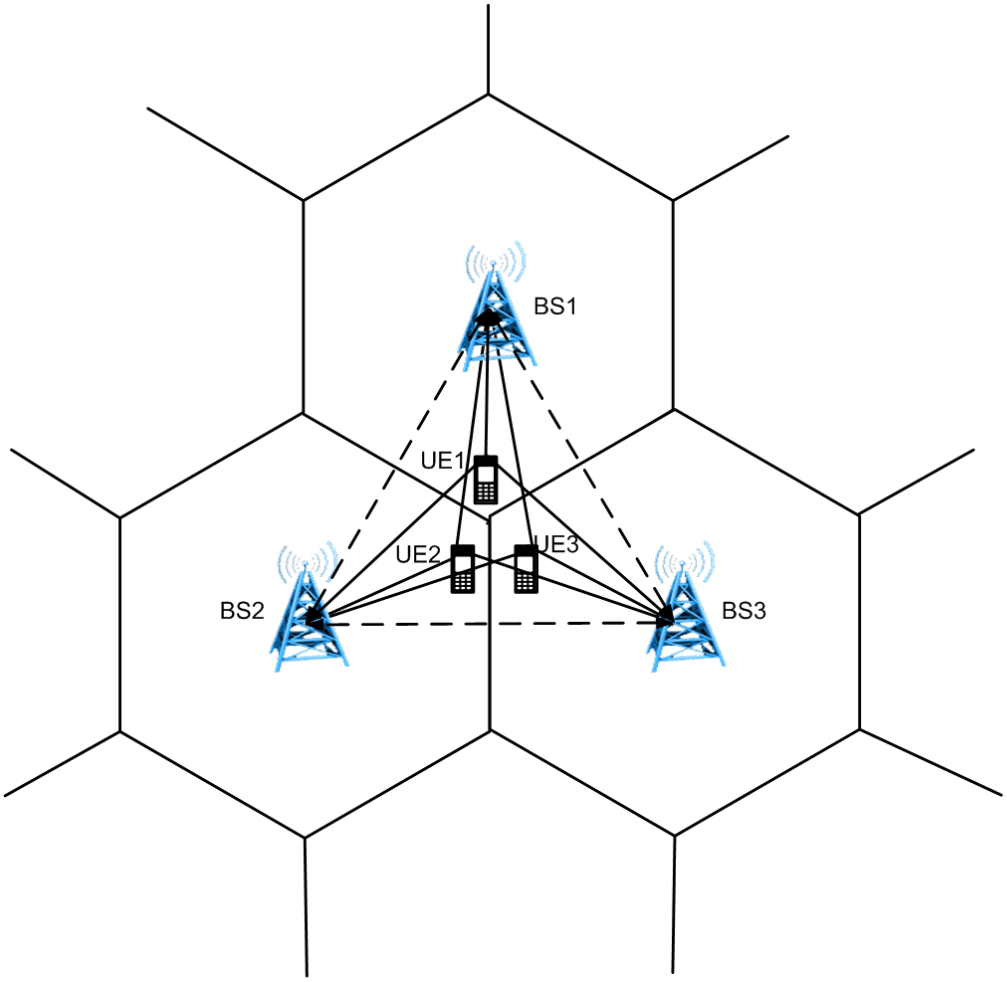

Fig. 3.8 SISO-CoMP Cellular network with 3 cell edge users

$$\text{Scenario 2: } y_n(i) = H_{n,n}(i)x_1(i) + \underbrace{\sum_{\substack{k=1 \\ k\neq n}}^{3} H_{k,n}(i)x_k(i)}_{\text{Known Interferer}} + \underbrace{\sum_{k=4}^{M} \psi_k \phi_k(i) H_{k,n}(i)x_k(i)}_{\text{Unknown Interferer}} + n_n(i) \tag{3.23}$$

The parameters are adjusted for single user case and details are omitted due to brevity.

3.4.2 Robust Multi-User detection result

For simulation, we consider the cells with ISD of 1000m.20 UEs per cell are randomly dropped in every cell. For cells other than coordinating cells, one UE per operator is selected randomly. For coordinating cells, cell edge UEs are selected.

The other parameters are same as mentioned in Table 3.1.

Here, results are only for the central cell. The results for other cells also follow in the same manner and it is not shown explicitly. Fig. 3.9 demonstrates the performance of the proposed scheme for scenario 1 with $\epsilon = 0.3$ and SIR of 3dB. Simulation is carried out for various LLR generation model with and without LLR combining. It is evident from the figure that Gaussian LLR based approach floors approximately from 18dB. The same is true even after combining the Gaussian LLRs. The performance of CC LLR, CG LLR, and CL LLR at the eNodeB is much better than the Gaussian LLR. Robust LLR combining shows noticeable performance improvement in the single antenna CoMP system described. The BLER performance with all the three Robust LLR models are within 0.4dB. CL LLR outperforms the CC LLR and CG LLR. At BLER of 10^{-3}, the improvement of combined CL LLR is around 18dB as compared to BLER performance of CL-LLR based multiuser detector at eNodeB1. One important observation from the result is that, if SNR is above 22dB, Robust LLR without LLR combining itself is better than the performance of combined Gaussian LLR based approach.

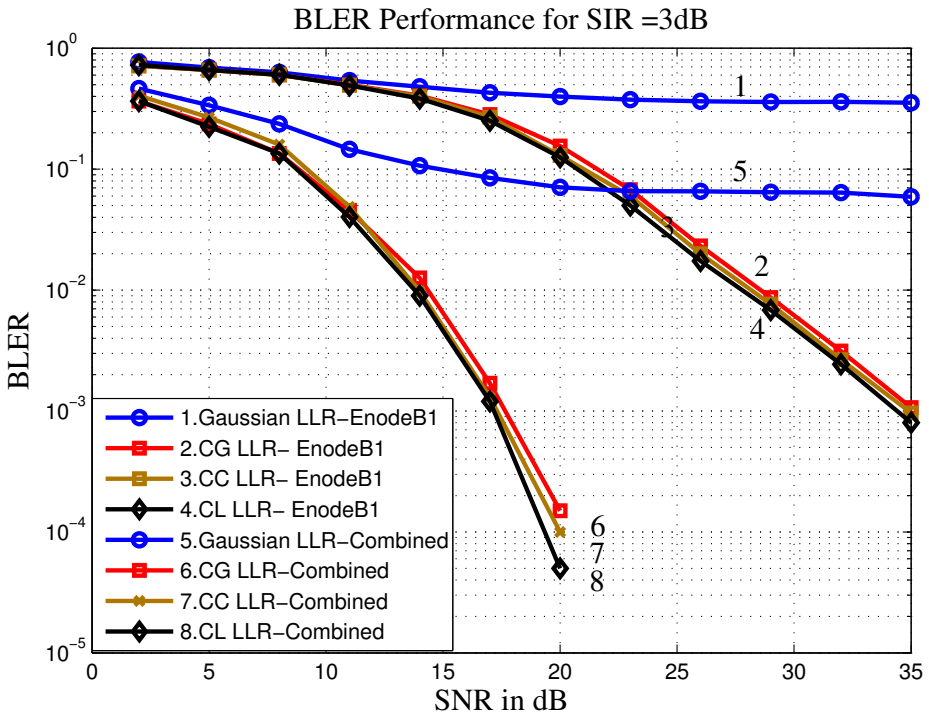

Fig. 3.9 BLER performance for scenario 1 with same ϵ for transmission scenario and LLR generation model

Fig. 3.10 compares the performance of the proposed scheme in Scenario 2

for various LLR generation models with and without LLR combining. The ϵ is set to 0.3 and SIR of 3dB is used for simulation. Unlike in Scenario 1, most of the subcarriers are getting affected by interference in Scenario 2. The result also dictates the same by showing the poor performance in Scenario 2 as compared to Scenario 1. As compared to Scenario 1, at each eNodeB, performance gap between the Robust LLR and Gaussian LLR is negligible in Scenario 2. One important inference from the result is that, all mentioned LLRs including Robust LLRs based technique floor at medium SNR onwards. Compared to Gaussian LLR, all mentioned Robust LLR performed better. Moreover, performance variation across Robust LLRs is noticeable in scenario 2. BLER performance of CL LLR is best among all the three models and performance of CC LLR is seen to be the worst.

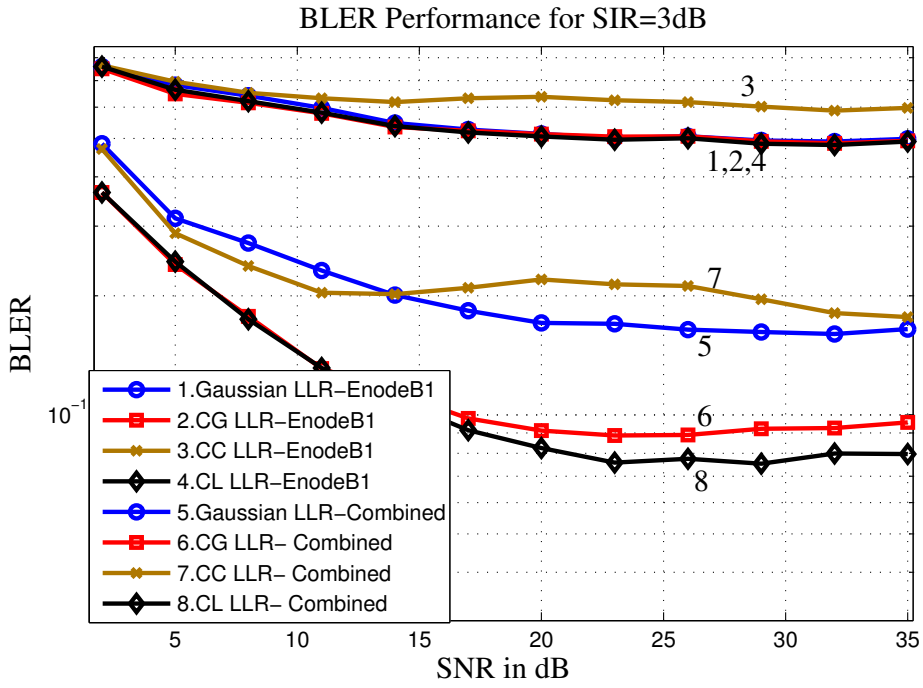

Fig. 3.10 BLER performance for scenario 2 with same ϵ for transmission scenario and LLR generation model

CHAPTER 4

LLR COMBINING FOR D2D COMMUNICATION

Device-to-device (D2D) communication enables direct communication between nearby UEs is an exciting and innovative feature of next-generation cellular networks. In principle, exploiting direct communication between nearby mobile devices will improve spectrum utilization, overall throughput, and energy efficiency. In low frequency application, it may be very cumbersome to have multiple receive chains on the UE side, given the 0.6m wavelength (assuming 500MHz of operation). Therefore, in order to provide some other form of spatial diversity on the downlink, we propose the use of D2D communications by LLR sharing. This is described clearly in this chapter, where in the typical scenario, the 2 UEs belong to different operators who share LLRs with each other. In other words, D2D cooperating user (secondary user) can be treated as virtual extension of antenna of the D2D user under consideration.

To facilitate D2D cooperation among UEs, it is required to perform device discovery. Device discovery can be performed similar to other known D2D schemes like LTE-Direct or WiFi Direct [28] or any other similar technology and this aspect is not considered in this thesis. Here, it is assumed that D2D pairing happens through minimum distance criteria where whichever UE is closest to the primary user is chosen as the secondary user. Cooperating user (noted as secondary user, in the vicinity of primary user) receives same transmitted signal and can provide this information (with or without processing) to primary user which in turn can apply any of the diversity techniques (like EGC, MRC etc..) to improve signal reception. Secondary user may pre-process and send information so as to reduce overall bandwidth requirement over D2D link. Here, it is important to note that D2D link bandwidth is typically much lower. Secondary user can process and send LLR information to primary user in two options. (i) LLR information sent for every block/frame or (ii) as and when requested by primary user. In (i) D2D

link bandwidth requirement is very high and in (ii) there is delay in receiving LLR information and UE needs to process information by storing own LLR information. When primary user target BLER is low (typical 0.01 to 0.001), the amount of processing required for D2D link is not high.

4.1 System Model And Device Architecture

We consider a 19 cell model for the analysis of the proposed technique where performance is monitored at the centre cell. An illustration is given in Fig. 4.1 The parameters are similar to the uplink, except the fact that devices are com-

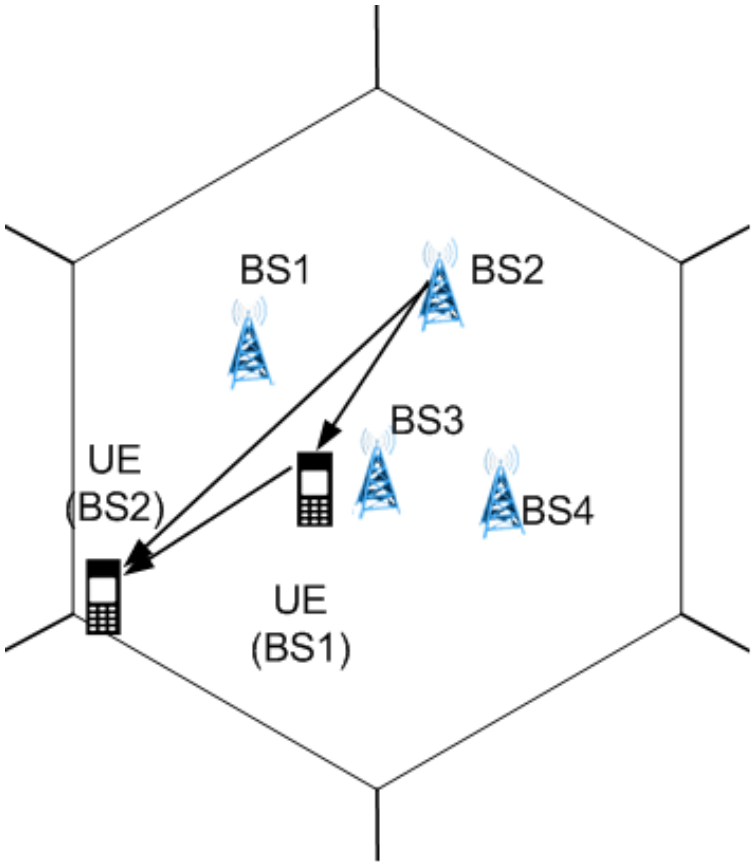

Fig. 4.1 System Model for D2D communication

municated via wireless medium rather than via back-haul. The details related to shared spectrum and UE to eNodeB communication models are similar to uplink system model as mentioned in chapter 2 and omitted from further discussion due to brevity.

The received LLR information, from secondary user, at the primary user for

any i^{th} time instant can be represented as follows.

$$y_(i) = H(i)x(i) + n(i) \tag{4.1}$$

where $H_i = \sqrt{\alpha\beta\gamma}h(i)$ denote the instantaneous channel from primary user to secondary user. Here, α and β represent the path loss and shadowing fading from primary user to secondary user. Also γ indicates the transmitter power of secondary user on D2D transmitter, which is being adjusted to get the required SNR at the primary user. The element h is an independent and identically distributed complex Gaussian random variable with zero mean and unit variance. $x(i)$ is symbol from unit modulus constellation. $n_n(i)$ denotes the additive white complex Gaussian noise with zero mean and variance σ^2. Note that interference term is not considered in the D2D link by having strict frequency management plan assumption.

A detailed block diagram of the envisaged user device is shown in Fig. 4.2. The diagram which includes RF front end, ADC and Band Pass Filters, and provides the IQ baseband data to both the LLR computational block and D2D receiver block. LLR computational block is responsible for computing the LLR for multiple eNodeBs based on the method described in Uplink LLR computation technique. Subsequently channel decoding will be performed and checksum is extracted to verify the block error. In case of error free block, LLR combiner will be bypassed and the information bit is given for further processing. In case of Block error, LLRs will be received from secondary user on request basis. After the reception of LLR from secondary user, LLRs will be combined and given to the channel decoder for extracting information bit. LLR buffer stores the quantized LLR of other eNodeBs for different operator and sends the LLR based on the request from other users.In D2D transmitter block, initially CRC will be appended on each block of quantized LLRs. Channel coding and bit interleaving will be performed on the this block and subsequently mapped to symbol constellation and given to Tx Antenna. On reception, BPF is responsible for extracting the secondary user data from the ADC output. LLRs will be computed based on the received data and turbo decoding will be performed to extract the bit stream. If the received block is error free, data will be given to LLR combiner block. In the current system model, it is assumed

that perfect D2D channel estimate is available for LLR computation block and only QPSK is used for modulation.

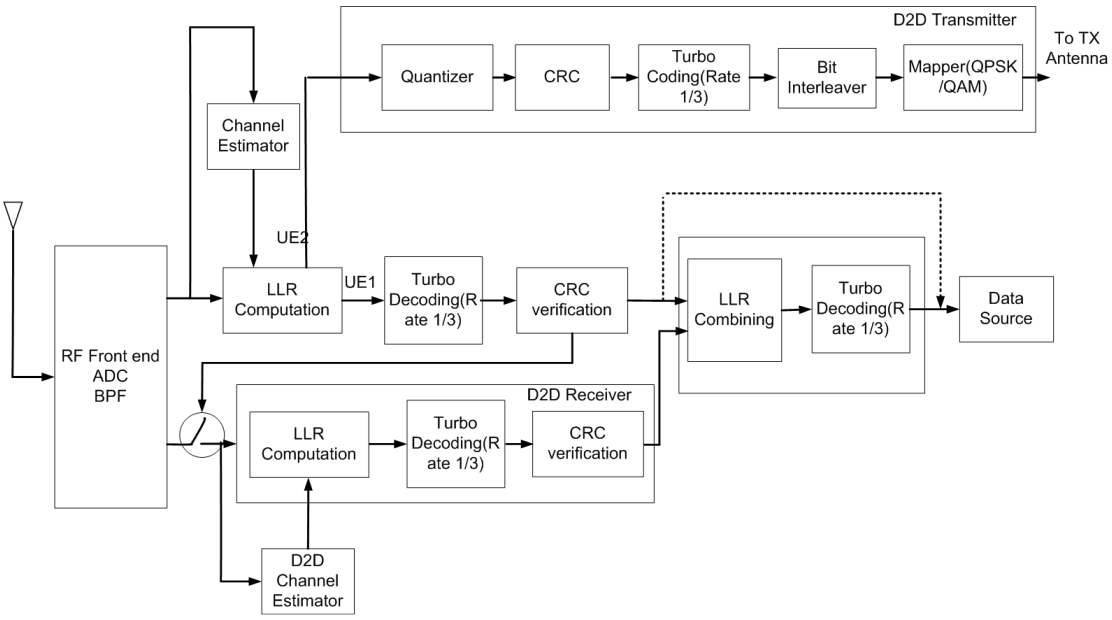

Fig. 4.2 UE block diagram for D2D communication

4.2 Simulation Result

Simulation is carried out to analyse the performance of the proposed technique for D2D communication. Simulation parameters are kept similar uplink processing as in chapter 2. Fig. 4.3 demonstrates the performance gain due to user LLR combining through D2D communication for various SNRs in the D2D chain. For simulation, secondary user is kept near to eNodeB where primary user is attached. The BLER performance also dictates the same by having a better performance as compared to primary user. It is evident from figure that the ideal LLR combining provides the gain of about 8-9 dB for the target BLER of 0.01. It is also observed that, combining without checking the block error at the primary user can cause a small deterioration in the performance. Another fact from the result is that as the D2D link quality improves, the performance of the combiner also enhances.

Fig. 4.4 demonstrates the performance of the LLR combiner with quantized LLRs. The SNR in the D2D chain is kept as 30dB for the simulation. It is observed that, there is no significant difference from ideal LLR to 3 bit uniformly quantized LLR. Note that the simulation scenario and the number of iterations for

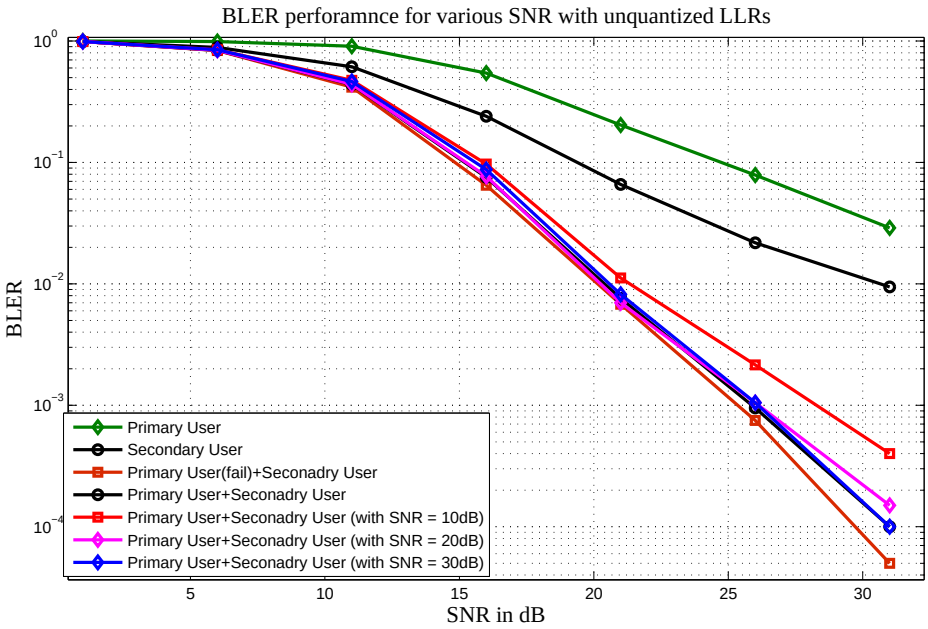

Fig. 4.3 BLER performance with LLR combiner for various SNRs

the BLER generation are different for generating Fig 4.3 and Fig. 4.4 and hence, direct comparison of these figures are not relevant.

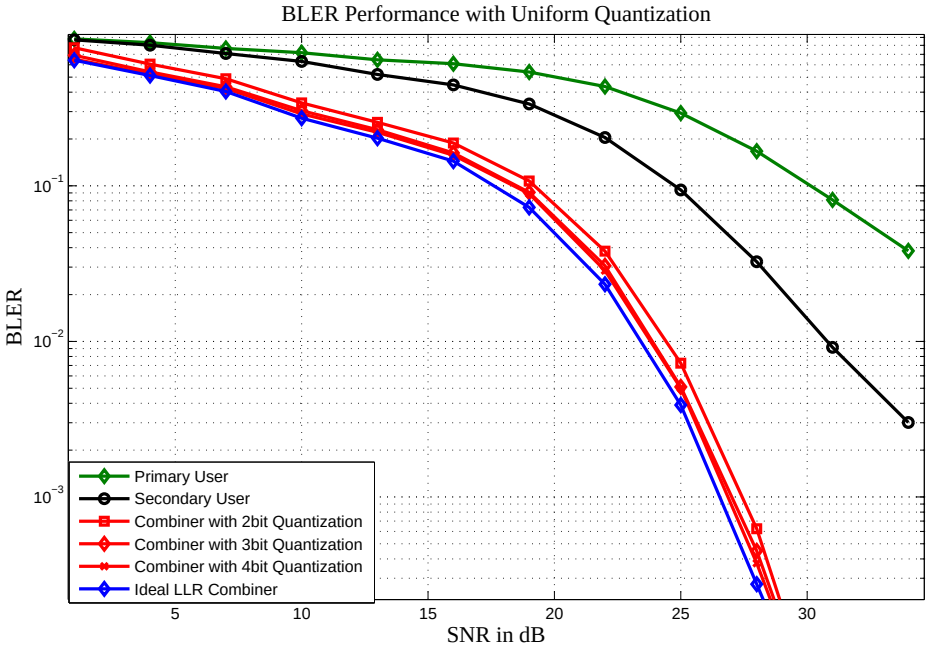

Fig. 4.4 BLER performance with LLR combiner with uniform quantization of LLRs

CHAPTER 5

5G WAVEFORM PERFORMANCE STUDIES

Digital modulation is the process of representing binary information using segments of different sinusoidal waveforms. It is classified into two, (i) Single-Carrier Modulation, and (ii) Multi-Carrier Modulation. Single-carrier modulation techniques use only one sinusoidal wave at all times, while in the multi-carrier modulation techniques, several sinusoidal waves are transmitted simultaneously. In our work, we analysed DFT-s-FDM and Zero-tail DFT-s-FDM as the single carrier waveform candidates and multi carrier waveform candidates are CP-OFDM, OFDM-WOLA, FBMC, GFDM and UFMC. The detailed block diagrams are given in appendix. The performance metric used for analysis are PAPR, PSD, and Time-Frequency Efficiency. Also, a comparison table is provided from the understanding about multiple waveforms from the literatures.

For the analysis purpose, LTE parameters with 10MHz of channel bandwidth is used. The parameters are given in Table 5.1. For waveforms, other than specified in LTE, values are considered in such a way that fair comparison with CP-OFDM (waveform for LTE) is ensured.

Table 5.1 Simulation parameter for waveform analysis

Sl No	Attribute	Value
1	Bandwidth[MHz]	10
2	Number of Resource block	50
3	Number of occupied subcarrier	600
4	FFT size, N	1024
5	Sample Rate[MHz]	15.36
6	CP length	73
7	Sub carrier spacing[KHz]	15
8	Guard Subcarrier(GS)	Lower GS: n $\in$ {0 to 212} Upper GS: n $\in$ {812 to 1024}

5.1 Peak to Average Power Ratio

The PAPR is defined on the base-band samples at the Tx DAC input as follows:

$$PAPR = \frac{\max |x(\tilde{k}, m)|^2}{\frac{1}{S \times N} \sum_{k=1}^{S} \sum_{m=1}^{N} |x(\tilde{k}, m)|^2} \tag{5.1}$$

where $x(\tilde{k}, m)$ denotes m^{th} the baseband samples for the k^{th} symbol, S denotes the total number of samples considered, and N represents the number of samples in one symbol. The PAPR for all the waveforms are shown in Fig. 5.1

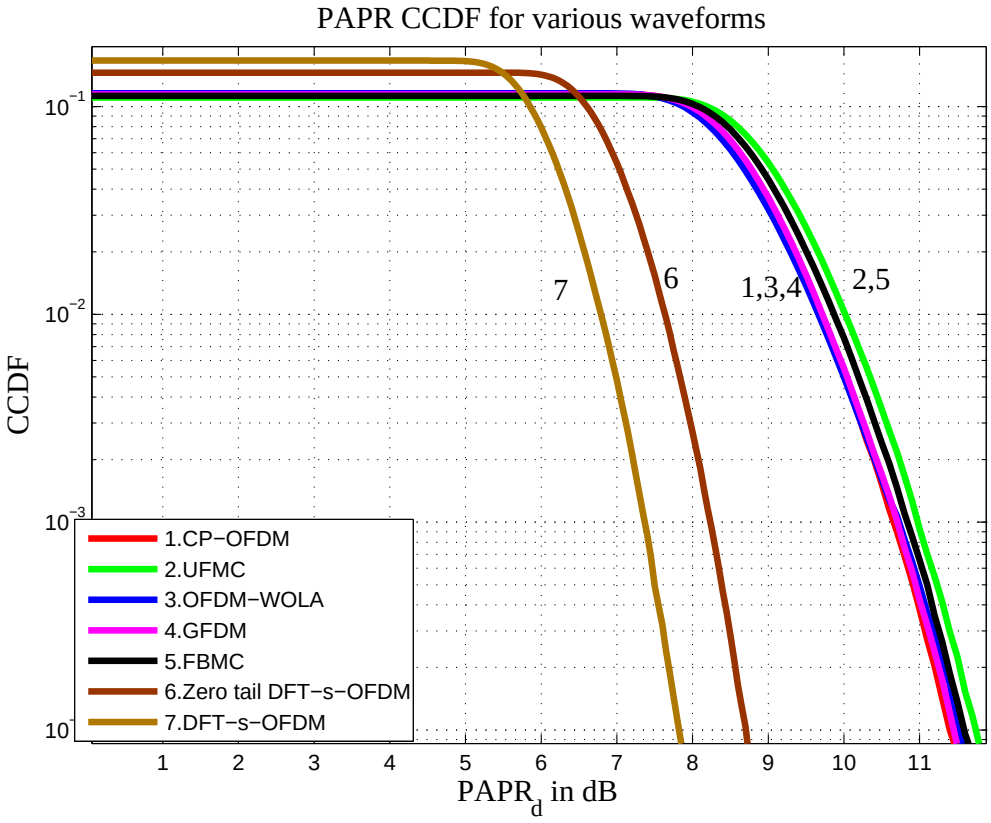

Fig. 5.1 PAPR for different waveforms

PAPR for all the multicarrier waveforms are almost similar. DFT-s-OFDM is seen to be the best performed waveform with respect to PAPR performance. The performance of zero tail DFT-s-OFDM is between DFT-s-OFDM and multicarrier waveforms.

5.2 Power Spectral Density

Out of Band emission is the one of the important parameter for the waveform selection and PSD is used for measuring OOB. PSD for the baseband sample is formulated as

$$P(f) = \lim_{T\to\infty}(\frac{1}{T}E\{|F\{x_T(t)\}|^2\}) \tag{5.2}$$

where $x_T(t)$ is the transmit signal that is truncated to the interval (-$\frac{T}{2}$, $\frac{T}{2}$). The number of guard subcarriers required in the transmitter block is selected based on the acceptable interference level on the adjacent channel and the power power spectrum of the chosen waveform. Therefore, the spectral efficiency is directly depending on the power spectrum of the selected waveform. PSD is also play a major in the Time-Frequency efficiency analysis of the waveform. The PSD for all the waveforms under consideration are given in Fig. 5.2.

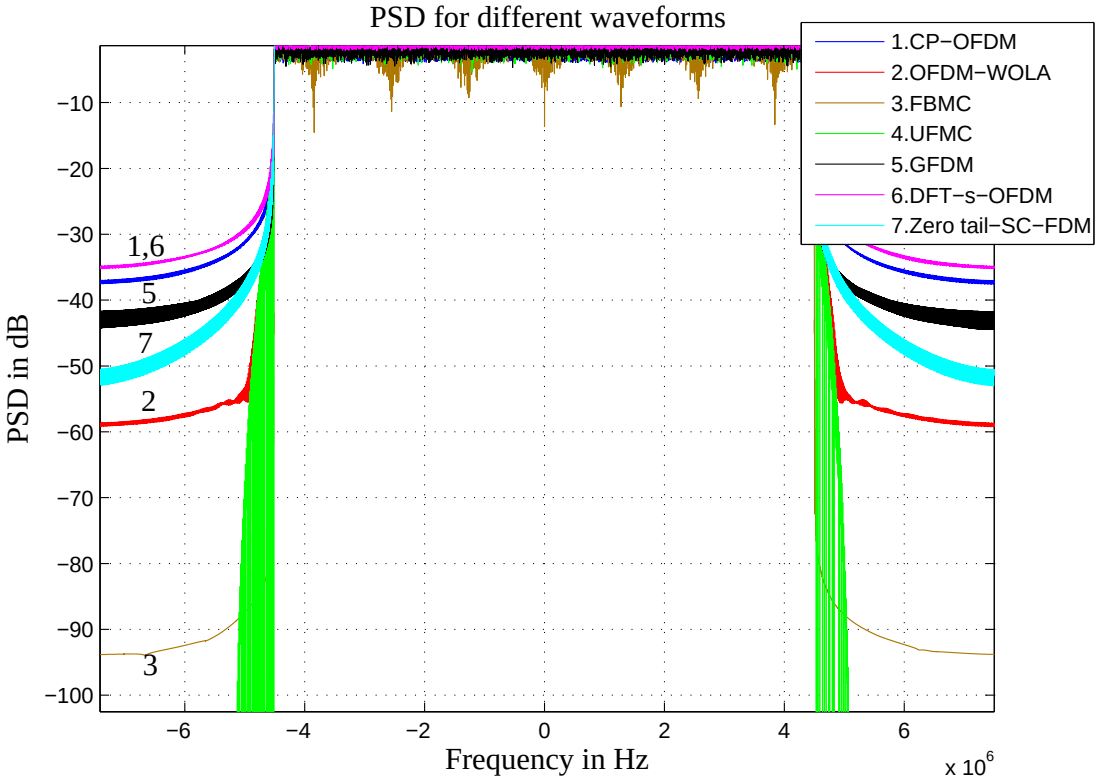

Fig. 5.2 PSD for different waveforms

From the figure, it is evident that the PSD of CP-OFDM and DFT-s-OFDM is very poor. This is due to the inherent rectangular pulse shaping in the FFT block of CP-OFDM and DFT-s-OFDM. The result also shows that guard band

requirement of these two waveforms are very high and thus, frequency domain efficiency will be very poor. Out of 660 usable subcarriers, 60 subcarriers are occupied as guard subcarriers which is 10% of the total available spectrum. For the aforementioned remark, it is assumed that acceptable interference level is -30dB. Compared to CP-OFDM, GFDM is performed better where Raised Cosine (RC) pulse shaping filter was used. Other candidate as the pulse filters is Root RC. As per literature, performance can be further enhanced by introducing time domain windowing on the digital samples which goes to Tx-DAC. From the result, an important observation is OOB performance of zero tail DFT-s-OFDM is much better as compared to CP-OFDM and DFT-s-OFDM. In order to make the fair comparison, CP length in CP-OFDM and number of low energy samples in Zero tail DFT-s-OFDM are kept same. The PSD performance of zero tail DFT-s-OFDM is mainly depends on the number of zeros used in the DFT block of the transmitter. As the number of zeros keeps increasing, OOB performance improves but the time domain efficiency reduces.

For OFDM WOLA, it is noticed that OOB suppression is substantially better than the CP-OFDM. Moreover, filtering based approach allows the asynchronous users in the network which alleviates the synchronization requirements. Again, the performance will be varied with different filter response. With respect to OOB, performance of FBMC is seen to be the the best among all the waveforms considered. The transition band of FBMC is extremely small and hence one subcarrier is sufficient as guard subcarrier. Also, FBMS allows asynchronous users in the network and between users, one subcarrier will be sufficient as guard subcarrier whereas in LTE (which uses CP-OFDM), it is 66! UFMC is also seen to be performed extremely well as compared to CP-OFDM. Similar to OFDM-WOLA and FBMC, UFMC also supports asynchronous operation because of the filtering approach and the better OOB performance. PSD of UFMC depends on the filters used for each resource block. In this work, we considered chebyshev filter and order of the filter is adjusted such that fair comparison with CP-OFDM is ensured.

5.3 Time-Frequency Efficiency

The time-frequency efficiency R_{TF} is defined as follows

$$R_{TF} = R_T.R_F = \frac{L_D}{L_D + L_T}.\frac{N_U}{N} \tag{5.3}$$

R_T is the efficiency in time direction relating the information carrying body (L_D) of the burst to its overall length including the tails (L_T). Here, the use of a cyclic prefix and the lengths of the filters are of relevance. Also,R_F is the efficiency in frequency direction relating the number of usable subcarriers N_U (i.e. excluding guards) to the overall number of subcarriers N within the usable band.

The time efficiency is characterized by the ratio of the length of the information carrying body of the transmitted burst to its overall length. If we assume the burst to contain M multicarrier symbols (each comprising N samples), we get:

$$L_D = MN \tag{5.4}$$

Regarding the tails, each waveform differ as follows:

$$\begin{aligned}
L_{T,CP-OFDM} &= ML_{CP} \\
L_{T,GFDM} &= L_{CP,GFDM} \\
L_{T,FBMC} &= (K - \frac{1}{2})N \\
L_{T,UFMC} &= M(L-1) \\
L_{T,OFDM_WOLA} &= ML_{CP} \\
L_{T,DFT-s-OFDM} &= ML_{CP} \\
L_{T,ZerotailDFT-s-OFDM} &= M(N_l + N_u)
\end{aligned} \tag{5.5}$$

where K is the overlapping factor, N_l, and N_u are lower and upper low energy samples in Zero-Tail DFT-s-OFDM. Also L_{CP} indicates the number of samples used for CP, L indicates the filter tap. As indicated in the above equations, for waveforms other than FBMC, and GFDM, L_T is proportional on the number of symbols in the burst.Thus, those waveforms are burst independent while computing the time frequency efficiency. For GFDM, irrespective of number of symbols

per burst,$L_{CP,GFDM}$ samples will be appended as CP for the whole block. For FBMC, the overlapping factor K and the number of samples per multicarrier symbol are the relevant quantities. An illustration of burst dependency of FBMC is given in Fig. 5.3 where two scenarios are described. Except number of symbols per burst, all other parameters are kept constant for simulation. It is evident from the figure that for short burst, percentage of samples occupied for filter ramp up and ramp down is huge whereas for long burst, it is less. While being advantageous for long bursts, this waveform is not favourable for very short burst transmissions.

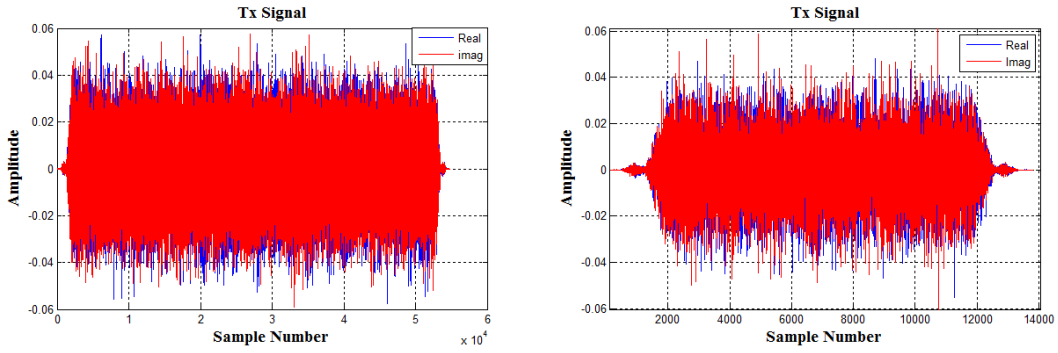

(a) Burst 1 (b) Burst 2

Fig. 5.3 Time domain FBMC waveform

Frequency domain efficiency is directly obtained from the PSD of the waveform. In Fig.5.2, it is evident that,if we allow -30 dB as the acceptable interference level, number of guard subcarriers required for the waveforms will be less as compared to CP-OFDM and DFT-s-OFDM. A detailed illustration is given in Fig 5.4 by taking UFMC as the waveform candidate. The highlighted region accommodate useful subcarriers in UFMC whereas, these are guard subcarriers for CP-OFDM.

From PSD, Table. 5.2 is derived which indicates the number of usable subcarriers for each waveform.

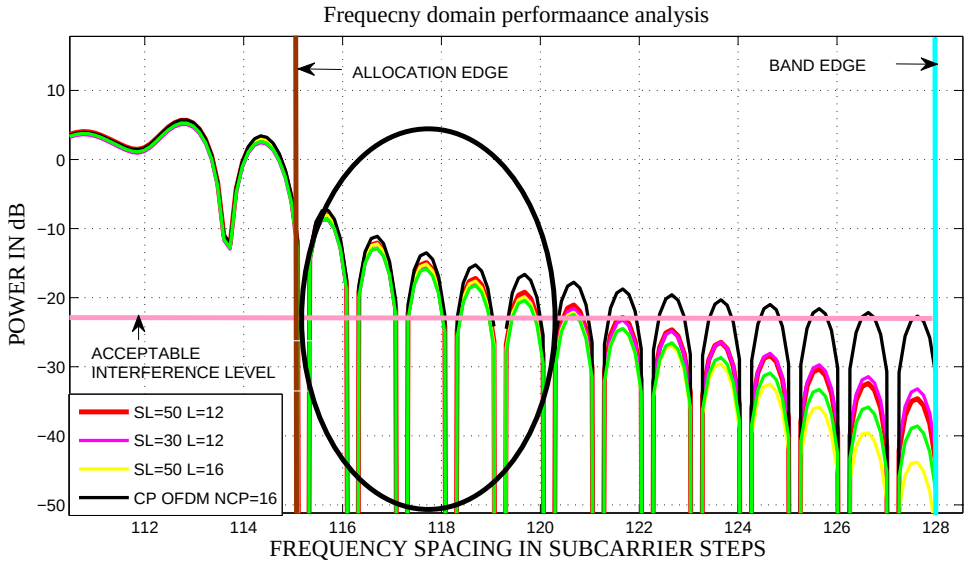

Fig. 5.4 Frequency Domain performance of UFMC

Table 5.2 Number of usable subcarriers for different waveforms

Sl No	Waveform	Number of usable subcarrier(N_U)
1	CP-OFDM	600
2	OFDM-WOLA	648
3	GFDM	626
4	FBMC	664
5	UFMC	646
6	DFT-s-OFDM	600
7	Zero Tail DFT-s-OFDM	640

Combining the time and frequency results, Fig. 5.5 compares burst independent waveforms CP-OFDM, DFT-s-OFDM, Zero-Tail DFT-s-OFDM and UFMC with respect to their time-frequency efficiency. For UFMC , various filter settings are considered for analysis and the details are given in Table 5.3.

Table 5.3 Filter parameters and usable subcarriers for UFMC

SideLobe / Length	SL=30dB	SL=40dB	SL=60dB	SL=90dB
L=40	650	648	646	642
L=60	654	652	650	648
L=80	658	656	654	652
L=100	660	660	658	654

The x-axis in Fig. 5.5 corresponds to the length of the filter (L) or the CP-length (LCP). The black vertical line reflects the design used by LTE (normal CP mode). OFDM-WOLA, UFMC and Zero Tail DFT-s-OFDM outperform CP-OFDM for any setting by about 10%.

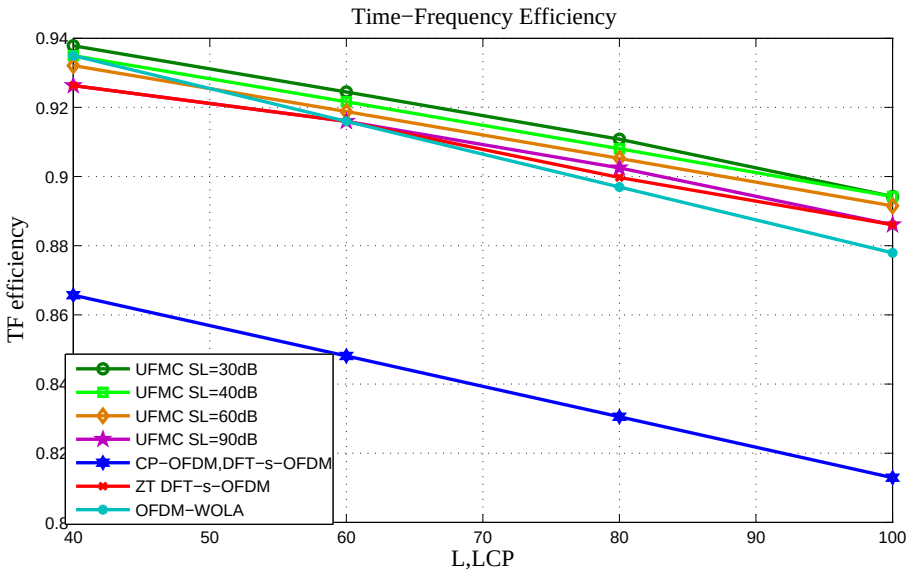

Fig. 5.5 Time-Frequency for burst dependent waveforms

Fig. 5.6 compares burst interdependent waveforms FBMC and GFDM with CP-OFDM and UFMC waveforms where filter sidelobe attenuation of UFMC is set to 60 dB. Overlapping factor K for FBMC is set to 4. The independence of the performance of a system applying OFDM or UFMC on burst is obvious from the figure. UFMC outperforms OFDM of about 10 % and brings additional benefits such as higher robustness to time and frequency misalignments and improves spectral properties. FBMC is very efficient with long bursts. However, the Time-Frequency efficiency degrades significantly in case of small burst as L_T does not

scale with burst for FBMC in contrast to UFMC and CP-OFDM. Time-Frequency efficiency of GFDM is also showed similar behaviour to FBMC, where waveform is suitable mainly for large burst.

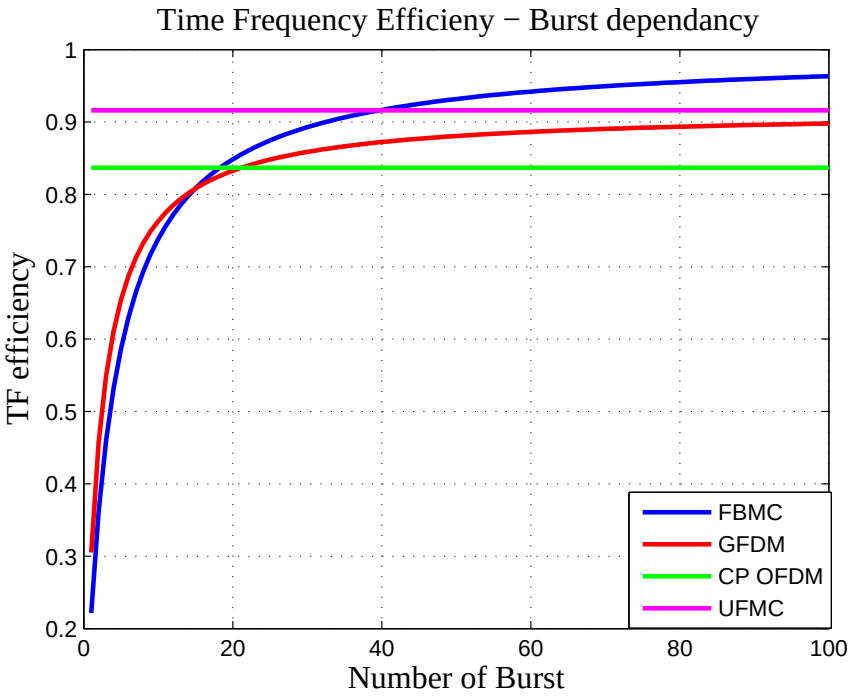

Fig. 5.6 Time-Frequency Efficiency for burst independent waveforms

5.4 Comparison Table for multicarrier waveforms

Table 5.4 Waveform Comparison Table

Attribute	CP-OFDM	FBMC	UFMC	GFDM	OFDM-WOLA	DFT-s-OFDM	ZT-DFT-S-OFDM
PAPR	Similar for all					Very Good	Good
Out of Band Interference	Low	Very Good	Very Good	Low (with out windowing)	Good	Low	Good
Receiver Complexity	Simple	Complex	Medium	Complex	Simple	Simple	Simple
Memory requirement	Low	High	Low	High	Low	Low	Low
Burst /Symbol operation	Symbol	Burst	Symbol	Burst	Symbol (2 symbols overlap)	Symbol	Symbol
Fragmented Operation	✗	√	√	√	√	✗	✗
Asynchronous Multiple Access	✗	√	√	√	√	✗	✗
Latency	1	K	1	M	2	1	1
Time Frequency Efficiency	Depends on no of users	Depends on no of symbol/burst	Depends on no of filter order	Depends on no of symbol/burst	Depends on no of symbol/burst	Depends on no of users	Depends on no of users
CP insertion	√	✗	✗	√	√	√	✗

CHAPTER 6

CONCLUSION

In this thesis, we considered the scenario of multiple operators simultaneously sharing the spectrum. We developed an efficient LLR computational method for multiple UEs in a eNodeB. Combining of LLRs from multiple eNodeBs with infinite precision representation of LLR is considered initially to get the upper bound for various digitization techniques. The result showed good improvement in the performance because of the receive and spatial diversity. Subsequently uniform quantisation and non uniform quantisation with clustering technique is described and analysed. Various result showed that 1.2 bit to 2.4 bit representation of the LLR is sufficient to achieve the performance within 0.3dB. Overall results demonstrated that the LLR combining with spectrum sharing allows us to operate the UE to eNodeB link in low BLER regime which in turn allows operating the UE either in low power mode or dense path loss scenario. As an extension of this work, the same concept was extended to downlink with uniform quantization technique. By using Device to Device (D2D) communication, performance enhancement of 7-8 dB was observed in downlink.

Subsequently, Robust LLR based approach was worked out in uplink by considering various noise model for LLR generation. The performance was analysed for different scenarios considering carrier aggregation and frequency management/reuse in a cellular network. We also demonstrated the performance of Robust LLR combiner for all mentioned models. Our current result indicates that the Gaussian-Laplacian model based approximation performs either better or close to the best of all the Robust LLR approaches considered. As an extension of this work, Robust LLR based technique was tried out in SISO CoMP system. The performance shows that the proposed method allows the scheduling of multiple users in the same time-frequency resource block, thus, enhancing sum-rate of the cellular network. The proposed scheme is highly useful in the low frequency, small cell scenarios (where more than a single antenna is not practical) and where modelling the strong interferers becomes a necessity.

As a part of improving spectral utilisation, different waveforms targeted for 5G cellular network was studied. Multiple waveforms CP-OFDM, OFDM-WOLA, FBMC, UFMC, GFDM, DFT-s-OFDM, and Zero Tail DFT-s- OFDM were analysed by using different performance metric like PAPR, OOB and Time-Frequency Efficiency. More over, a comparison study was carried out across waveforms.

APPENDIX A

STUDY ON 5G WAVEFORM CANDIDATES

Digital modulation is the process of representing binary information using segments of different sinusoidal waveforms. The waveforms are classified into two, (i)Single-Carrier Modulation, and (ii) Multi-Carrier Modulation. The details of the following waveforms given in this appendix. DFT-s-OFDM and Zero-tail DFT-s-OFDM are described as the single carrier waveform candidates and multi carrier waveform candidates are CP-OFDM, OFDm-WOLA, FBMC, GFDM and UFMC.

A.1 Cyclic Prefix-OFDM

The CP-OFDM waveform is the most widely used multi-carrier waveform in existing broadband wireless standards, including 3GPP LTE and IEEE 802.11. The block diagram for transmitter and receiver is given in Fig. A.1. The main functions in the transmitter including serial to parallel conversion, inverse DFT processing, parallel to serial conversion and CP insertion. In a receiver, the main functions are CP removal, serial to parallel conversion, DFT processing, and parallel to serial conversion. Additional efforts are required to handle the channel-fading effect and synchronization issues between the transmitter and the receiver. The main features of CP-OFDM waveform are:

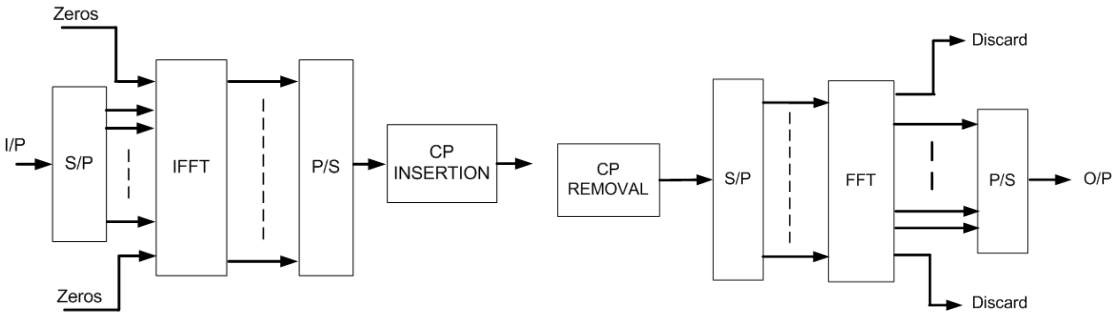

Fig. A.1 Modulator and demodulator for CP-OFDM

1. Efficient implementation using FFT/IFFT
2. High spectrum efficiency with the use of the CP over non flat channel
3. Simple Frequency Domain Equalization per subcarrier for non-flat channel
4. Dynamically allocate bandwidth to users

Even though CP-OFDM is simple and lot of attractive features as mentioned, the poor frequency location and extra overhead due to CP leads to the search for new waveforms. The poor frequency location is because of the inherent rectangular prototype filter in the CP-OFDM transmitter block. Moreover, PAPR is noticeably higher than the single carrier waveform, which is going to be a common issue with all multi-carrier waveforms.

A.2 OFDM-Weighted-Overlap-and-Add

In CP-OFDM, the rectangular prototype filter is replaced with a pulse with smooth edges on both sides results in better side lobe performance and hence, provides better frequency localization. In OFDM-WOLA, better frequency response is achieved by using a time domain windowing approach which add soft edges to the cyclic extension of CP-OFDM symbol. The transmitter and receiver block diagram is shown in Fig. A.2. Compared to CP-OFDM ,only difference is additional WOLA block in the transmitter and receiver chain and the overhead is still same as CP-OFDM.

Fig. A.3 provides transmit and receive windowing operation of the WOLA filter. In operation, input symbol-A is received from the output of IFFT block of the transmitter module. A preselected portion of the end of the the symbol-A is copied, weighed with left edge weighting function-B and appended to the beginning of the symbol-A as CP. Right edge weighting function-A can also be applied to the end of the symbol-A and the resulting waveform is shown in figure. WOLA filter is used to control the length and degree of edge rolloff of the transmit waveform derived from the IFFT input symbol. While in the reception, transmitted waveform has been captured and stored in the receive buffer. The received waveform is shortened to the FFT input length by first applying a weighted average

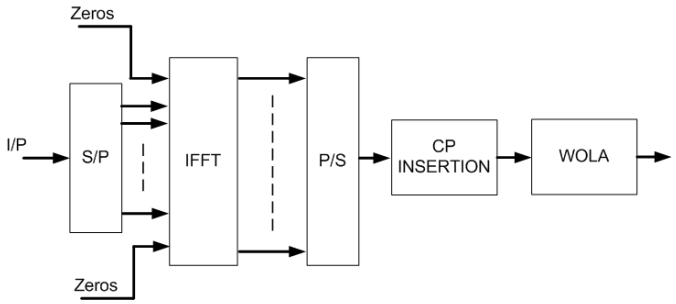

(a) Transmittter

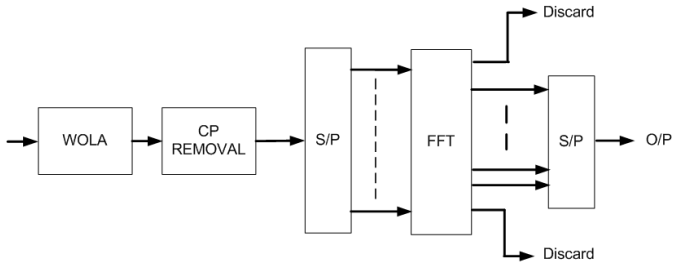

(b) Receiver

Fig. A.2 Modulator and demodulator for OFDM WOLA

window which may have a larger size than the FFT input length. Then, the edges of the weighted average output step can be overlapped and added. Finally, a segment within this output of a length equal to FFT input is selected for further processing.

In addition to applying WOLA at the transmitter to reduce the OOB leakage from the signal, we notice that WOLA can be similarly applied at the receiver to suppress other users interference as well. When users are asynchronous, the soft edges applied at the receiver help to reduce other user interference resulting from the mismatched FFT capture window

A.3 Filter Bank Multi Carrier

FBMC, based on filter bank theory, introduces filter banks to the OFDM system and discards the CP. Fig. A.4 presents a transceiver block diagram that is commonly used to depict an FBMC transceiver. This structure is also applicable to OFDM.

As shown in the diagram, each subcarrier is filtered by using a prototype filter. As compared to OFDM system, difference is especially in the transmitter

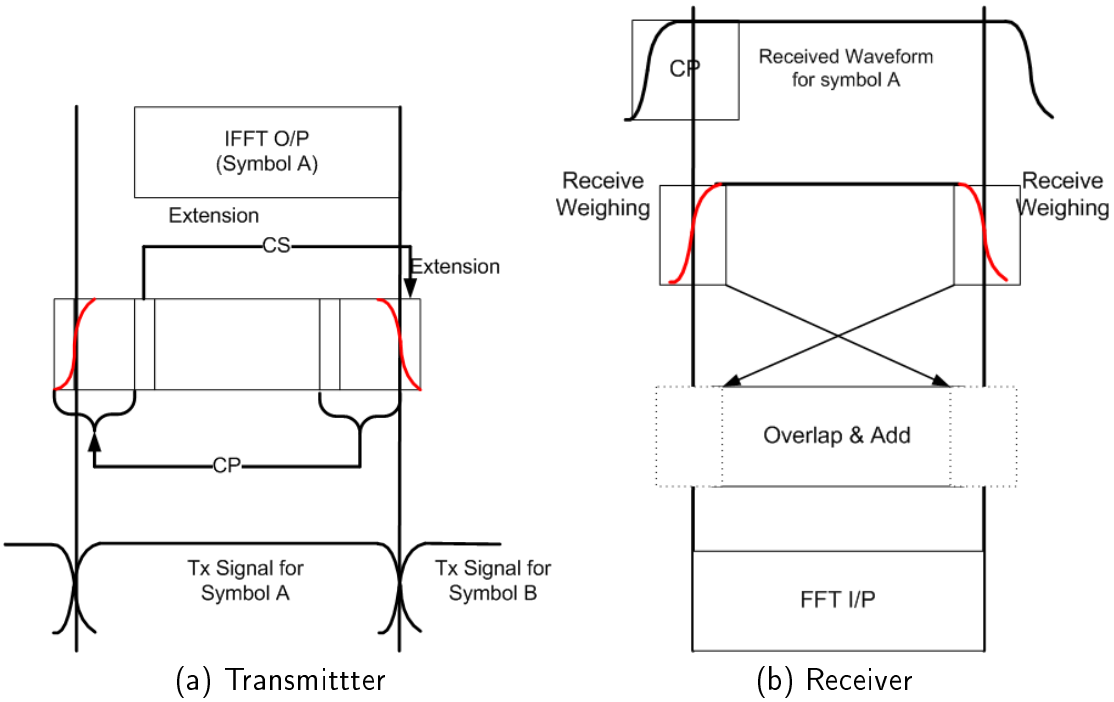

Fig. A.3 OFDM WOLA : Windowing operation on transmitter and receiver

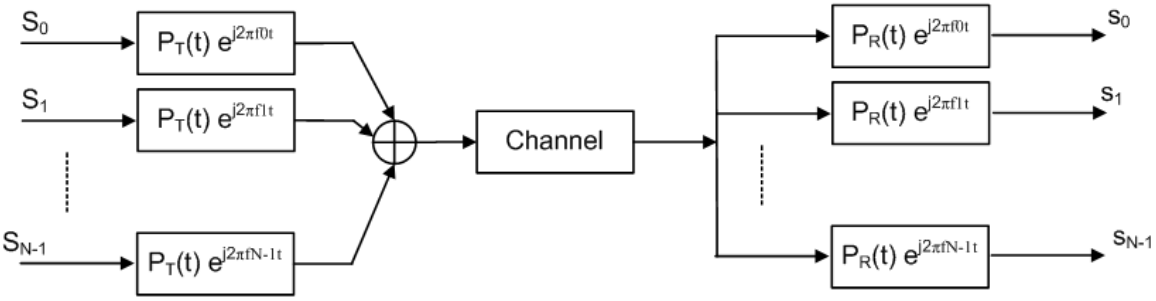

Fig. A.4 Modulator and demodulator for FBMC

and receiver prototype. In a conventional OFDM, these prototype filter in the transmitter is rectangular pulse of height one and width symbol duration,T. The receiver prototype filter is also a rectangular pulse of height one, but its width is reduced to T_{FFT} < T, where T_{FFT} =1/B, and B is the frequency spacing between subcarriers. In FBMC systems that are designed for maximum bandwidth efficiency, T=T_{FFT}= 1/B, however, the durations of filters are greater than T (usually, an integer multiple of T). Hence, in FBMC, the successive data symbols overlap.

The well-localized spectral property is achieved through optimizing the shape of the prototype filter through oversampled coefficients in frequency domain. Specif-

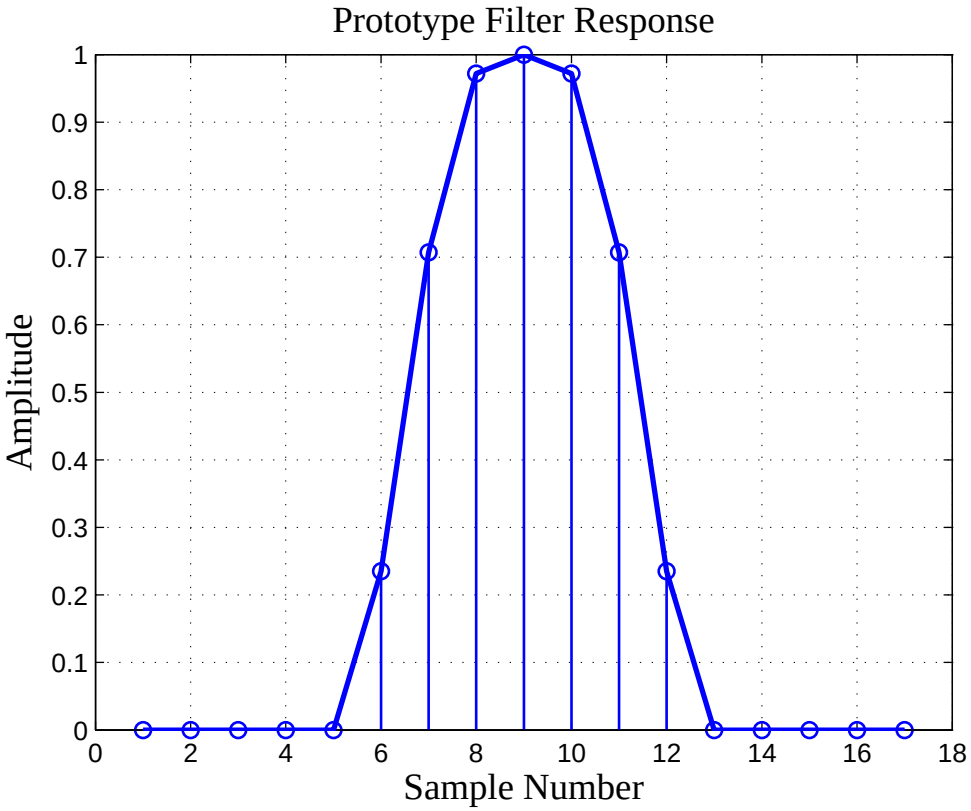

Fig. A.5 Prototype Filter response

ically, the oversampling factor K is denoted as the FBMC overlapping factor. Fig. A.5 shows an example prototype filter with in frequency domain with K=4, i.e. the interval between adjacent coefficients is 1/4 Δ_f, where $\Delta_f = \frac{1}{T}$ is the sub-channel spacing. The non-zero coefficients are specified in Table A.1.

Table A.1 FBMC prototype filter: Non-zero filter coefficients in frequency domain

H_{-3}	H_{-2}	H_{-1}	1	H_{-1}	H_{-2}	H_{-3}
0.235147	$\frac{\sqrt{2}}{2}$	0.97196	1	0.97196	$\frac{\sqrt{2}}{2}$	0.235147

Notice that FBMC waveform synthesis can be efficiently implemented based on polyphase filter network (PPN) as shown in Fig. A.6. The fundamental change is the replacement of the OFDM with a multicarrier system based on filter banks, i.e. IFFT plus CP insertion is replaced by the synthesis filter bank while CP removal plus FFT is replaced by the analysis filter bank as shown in Fig. A.6. However, modulation and demodulation in FBMC generally have higher complexity than other OFDM waveforms even in systems without MIMO.

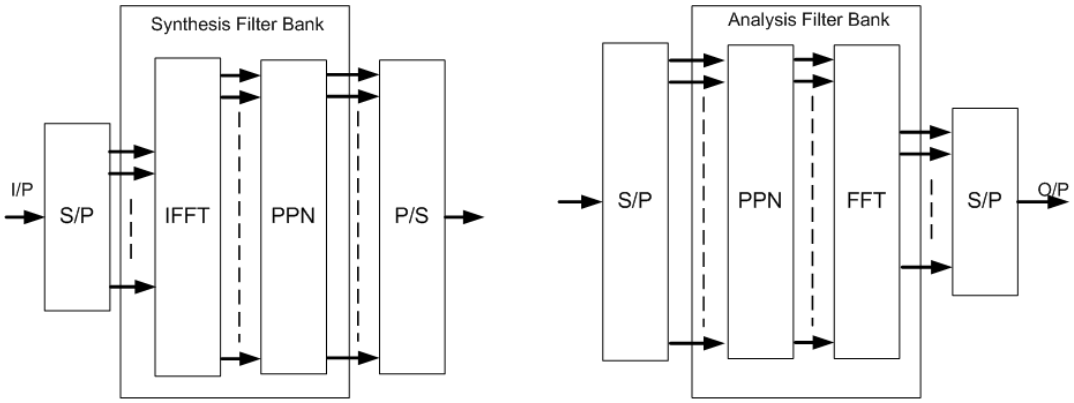

Fig. A.6 FBMC transciver in a multirate context

A.4 Universal Filtered Multi Carrier

While FBMC performs a per-subcarrier filtering, filtered OFDM applies a filtering operation for the entire frequency band. The UFMC solution shown in Fig. A.7 is a generalization of filtered OFDM and FBMC. The time-domain transmit vector

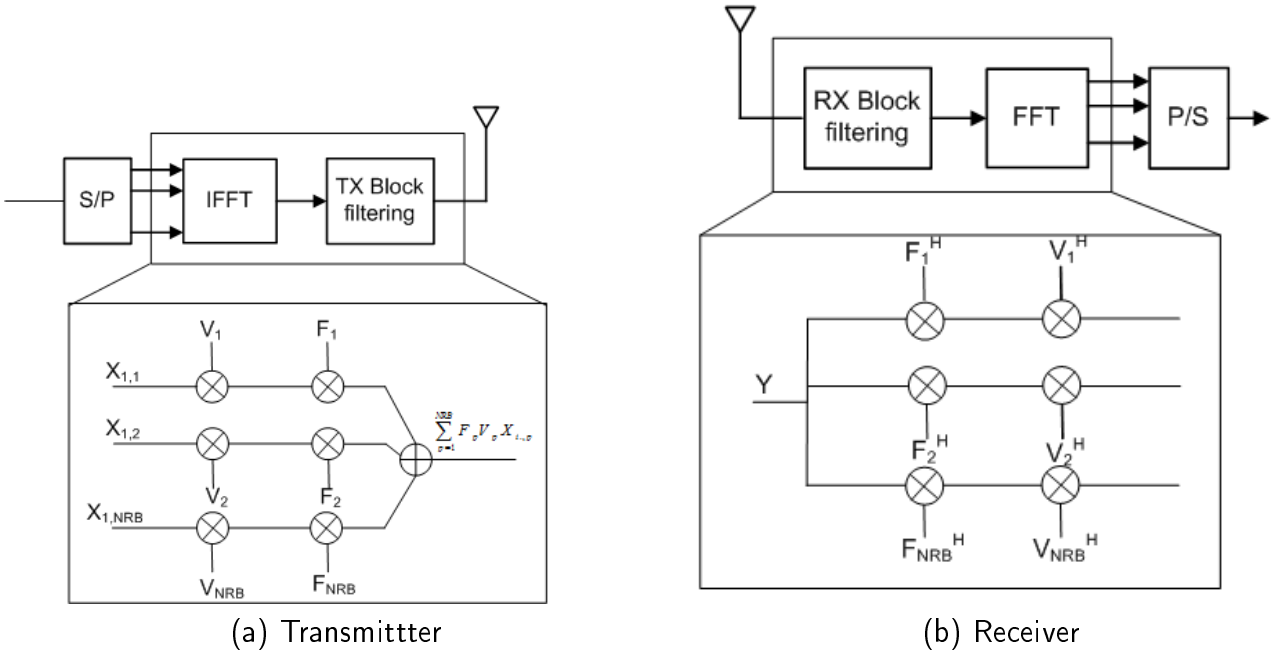

Fig. A.7 Modulator and demodulator for UFMC

for a particular multicarrier symbol of user k is the superposition of the sub-band

wise filtered components, with filter length L and FFT length N:

$$\underset{[N+L-1\times 1]}{X_k} = \sum_{i=1}^{B} \underset{[(N+L-1)\times N]}{F_{ik}} \underset{[N\times n_i]}{V_{ik}} \underset{[n_i\times 1]}{s_{ik}} \tag{A.1}$$

For each of the B subbands, indexed i, the n_i complex QAM symbols are transformed to time-domain by the IDFT matrix V_i. V_i includes the relevant columns of the inverse Fourier matrix according to the respective sub-band position within the overall available frequency range. FV_i is a Toeplitz matrix, composed of the filter impulse response, performing the linear convolution. Note that there is no time overlap between subsequent UFMC symbols. The symbol duration of N+L-1 samples is generated by the filter length and the FFT size.

A.5 Generalised Frequency Division Multiplexing

GFDM is based on the modulation of independent blocks, where each block consist of a number of subcarriers and subsymbols. The subcarriers are filtered with a prototype filter that is circularly shifted in time and frequency domain. This process reduces the OOB emissions, making fragmented spectrum and dynamic spectrum allocation feasible without severe interference in incumbent services or other users. The subcarrier filtering can result in non-orthogonal subcarriers and both inter-symbol interference (ISI) and inter-carrier interference (ICI) might arise. Nevertheless, efficient receiving techniques can eliminate this interference. The details of the modulator and demodulator is given in Fig. A.8.

In a GFDM block, the overhead is kept small by adding a single CP for an entire block that contains multiple subsymbols. This benefit can be used to improve the spectral efficiency of the system. GFDM is confined in a block structure of MKsamples, where K subcarriers carry M subsymbols each, it is possible to design the time frequency structure to match the time constraints of low latency applications. Different filter impulse responses can be used to filter the subcarriers and this choice affects the OOB emissions and the SER performance

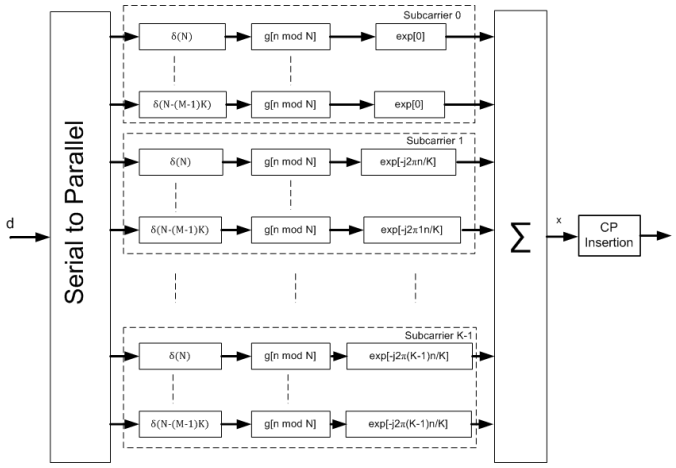

(a) Transmittter

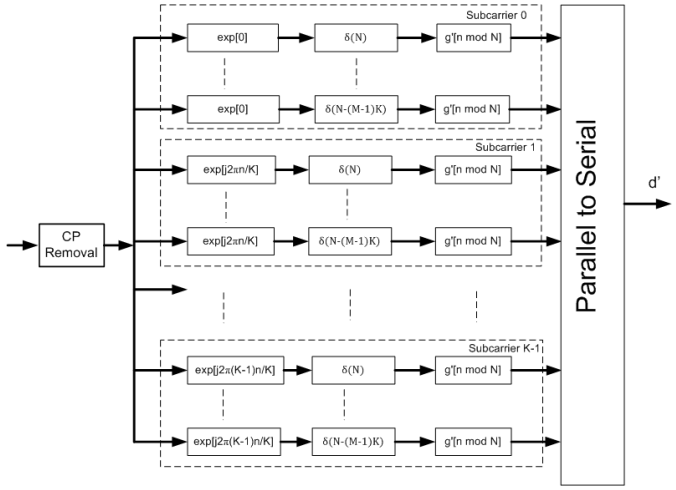

(b) Receiver

Fig. A.8 Modulator and demodulator for GFDM

A.6 DFT-spread-OFDM

DFT-s-OFDM is a multiple access technique that utilizes single carrier modulation, and frequency domain equalization. It has a similar structure and performance as OFDM. DFT-s-OFDM is currently adopted as the uplink multiple access scheme for 3GPP LTE. Transmitter and receiver structure for DFT-s-OFDM and OFDM are given in Fig. A.9. It is evident from the figures that DFT-s-OFDM transceiver has similar structure as a typical OFDM system except the addition of a new DFT block before subcarrier mapping. Hence, DFT-s-OFDM can be considered as an OFDM system with a DFT mapper. DFT output of the data symbols is mapped to a subset of subcarriers, a process called subcarrier mapping.

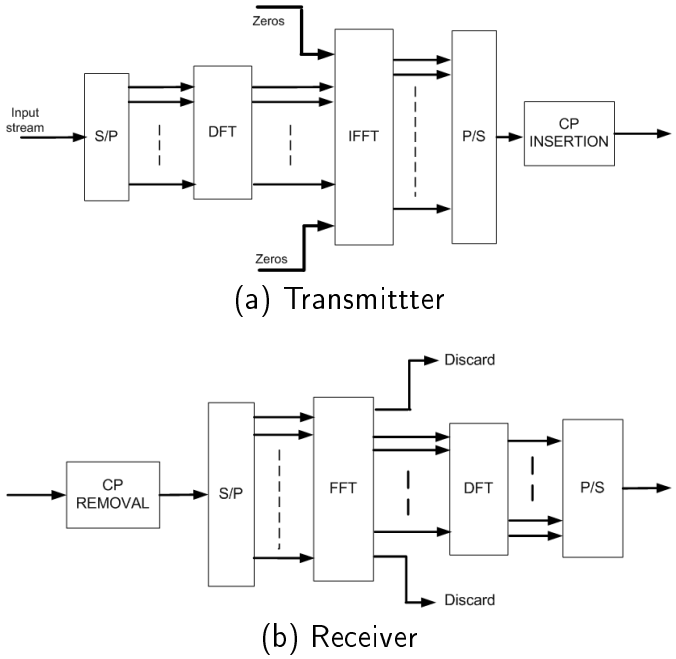

Fig. A.9 Modulator and demodulator for DFT-s-OFDM

The subcarrier mapping assigns complex valued DFT output samples as the amplitudes of some of the selected subcarriers. Subcarrier mapping can be classified into two types: localized mapping and distributed mapping. In localized mapping, the DFT outputs are mapped to a subset of consecutive sub-carriers thereby confining them to only a fraction of the system bandwidth. In distributed mapping, the DFT outputs of the input data are assigned to subcarriers over the entire bandwidth non-continuously, resulting in zero amplitude for the remaining subcarriers. A special case of distributed SC-FDMA is called interleaved SC-FDMA, where the occupied subcarriers are equally spaced over the entire bandwidth.

A.7 Zero-Tail DFT spread OFDM

The usage of zero-tail DFT-s-OFDM signals as an alternative to traditional CP-based DFT-s-OFDM modulation. Such signals are designed with the aim of decoupling the radio numerology from the channel characteristics by replacing the CP with a set of very low power samples (zero-tail) which are part of the IFFT output. This leads to the possibility of setting the overhead represented by the low power samples according to the estimated channel without compromising the numerology. Hence, the main change is that the regular cyclic prefix is replaced

by zero samples padded to the data input to the DFT precoding, as shown in Fig. A.10. Similarly in receiver, zeros will be discarded from the output of the DFT block. Note that the proposed solution is different from known zero padded

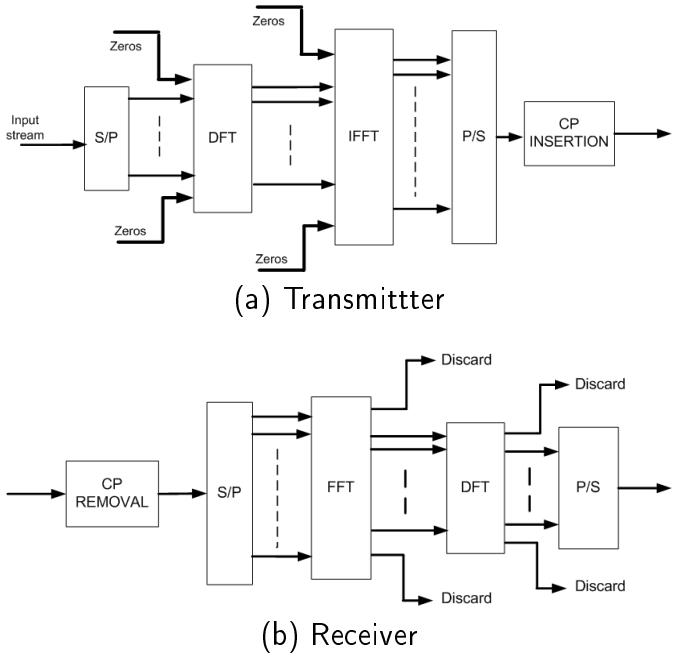

Fig. A.10 Modulator and demodulator for ZT DFT-s-OFDM

approaches (e.g., [29]), which replace the CP with zeros with the aim of improving robustness to the channel fades with a penalty in receiver complexity, since cyclicity at the receiver is partly lost. Here, it aims instead at a solution which preserves the orthogonality of the data subcarriers at the receiver. Such zero-tail waveforms have then the following advantageous properties:

1. Adaptivity to the estimated delay spread/propagation delay: The zero part,T_{s0}, can be set dynamically without modifying the system numerology. This allows to avoid the potential throughput losses or BLER increase due to an hard-coded CP. Delay spread can be estimated for instance from pilot sequences periodically sent, and T_{s0} set accordingly.

2. Coexistence with systems using different T_{s0} . Since the T_{s0} samples are part of the OFDM/DFT-s-OFDM symbol itself, systems operating over different types of channels can use the same numerology (e.g., symbol length). In case such systems are synchronized at both frame and symbol level, they can coordinate their transmission in order not to interfere each other. Moreover, even when simultaneously transmitting, they would generate mutual synchronous interference which can be suppressed by the IRC and SIC detectors, boosting the throughput performance.

3. The OOB leakage can be suppressed due to the zero padding, which smoothens the transitions between adjacent symbols.

4. Zero tail can potentially reduce the overhead associated with RF beam switch.

When comparing DFT-spread OFDM with zero-tail, it would seem there is a slight improvement in link performance with the zero tail guard optimization. However, in reality it is not sufficient to only change the CP or guard to handle all delay spreads, but the subcarrier spacing (and thus block length) should also be scaled to best address the delay spread and channel selectively. Therefore, for the same block size and subcarrier spacing, the zero tail guard optimization might only benefit up to 7%, if we consider the CP overhead in LTE. Moreover, there would be additional signalling overhead to support the added control loop complexity for zero-tail.

REFERENCES

[1] 3GPP, TR 36.819 "Coordinated Multi-Point Operation for LTE Physical Layer Aspects".

[2] J. Lee, Y. Kim, H. Lee, B. L. Ng, D. Mazzarese, J. Liu, W. Xiao, and Y. Zhou, "Coordinated multipoint transmission and reception in LTE advanced systems," Commun. Mag., IEEE, vol. 50, no. 11, pp. 44âĂŞ50, November 2012.

[3] T. Innovations, "LTE in a nutshell", White Paper, 2010.

[4] E. W. Jang, J. Lee, H.-L. Lou, and J. M. Cioffi, "On the combining schemes for MIMO systems with hybrid ARQ," IEEE Trans. Wireless Commun., vol. 8, no. 2, pp. 836-842, Feb. 2009

[5] D. Chase, "Code combining-a maximum-likelihood decoding approach for combining an arbitrary number of noisy packets," IEEE Trans. Commun., vol. 33, pp. 385-393, 1985

[6] R. Ratasuk, D. Tolli and A. Ghosh, "Carrier aggregation in LTE advanced", 2010 IEEE 71st Vehicular Technology Conf. (VTC 2010 Spring), pp. 1-5

[7] J H. Holma and A. Toskala, "LTE-Advanced: 3GPP Solutions for IMT Advanced",Wiley, 2012

[8] H. Holma and A. Toskala, LTE for UMTS: OFDMA and SC-FDMA Based Radio Access. Wiley, 2009.

[9] Asynchronous Multicarrier Communication : US Patent No:20150349987

[10] Schaich, F , " Filterbank Based Multi Carrier Transmission (FBMC)-evolving OFDM " , Wireless Conference (EW), 2010

[11] M. Bellanger, "FBMC physical layer: a primer, PHYDYAS" Jan 2010

[12] Vakilian,V.; Wild, T.; Schaich, F.; ten Brink, S.; Frigon, J.-F.,"Universal Filtered Multi-Carrier Technique for Wireless Systems Beyond LTE", 9th Int. Workshop on Broadband Wireless Access at IEEE Globecom-13, Atlanta, Dec. 2013

[13] Nicola Michailow, Ivan Gaspar, Stefan Krone, Michael Lentmaier, Gerhard Fettweis , "Generalized Frequency Division Multiplexing: Analysis of an Alternative Multi-Carrier Technique for Next Generation Cellular Systems", Vodafone Chair Mobile Communications Systems, Technische UniversitÂÍat Dresden, 01069 Dresden, Germany

[14] G. Berardinelli, F. M. L. Tavares, T. B. Sorensen, P. Morgensen and K. Pajukoski, "Zero-tail DFT-spread-OFDM signals", 2013 IEEE Globecom Workshops, pp. 229-234

[15] S. Caleri, M. Ergen, A. Bahai. "Channel estimation techniques based on pilot arrangement in OFDM systems", IEEE Trans. Broadcast., vol. 48.no. 3, pp. 223.229, sept. 2002

[16] F. 1. L. Baht, 1. Cocke and 1. Raviv, "Optimal decoding of linear codes for minimizing symbol error rate," IEEE Trans. Inf Theory, vol. 2, p. 284287, Mar. 1974

[17] J. Max, "Quantizing for minimum distortion", IEEE Trans. Inf. Theory, vol. 6, pp. 7-12, 1960

[18] W. Rave, "Quantization of log-likelihood ratios to maximize mutual information," IEEE Signal Process. Lett., vol. 16, no. 4,Apr. 2009.

[19] Laktyushkin Anton, Haechul Lee, Chaehag Yi, "An adaptive Log-likelihood Ratio compression algorithm for Downlink Shared Channel processing in LTE receiver," ISOCC 2013 Apr. 2009.

[20] 3GPP TS 36.211, "LTE; Evolved Universal Terrestrial Radio Access (E-UTRA); Physical channels and modulation" Release 10.

[21] Q. Li, R. Q. Hu, Y. Qian and G. Wu, "Cooperative communications for wireless networks: Techniques and applications in LTE-advanced systems", IEEE Wireless Commun., vol. 19, no. pp. 22-29, 2012

[22] A. Nosratinia, T. E. Hunter, and A. Hedayat, "Cooperative communication in wireless networks", IEEE Commun. Mag., vol. 42, pp. 74-80, 2004

[23] 3GPP, TR 36.819, "Coordinated Multi-Point Operation for LTE Physical Layer Aspects".

[24] 3GPP TS 36.300 V8.4.0, "Technical Specification Group Radio Access Network; (E-UTRA) and (E-UTRAN): Overall Description"

[25] S.-H. Sun, Q.-B. Gao, Y. Peng, Y.-M. Wang and L.-Y. Song, "Interference management through CoMP in 3GPP LTE-Advanced networks", IEEE Wireless Commun., vol. 20, no. 1, pp. 59-66, 2013

[26] S. Kalyani and K. Giridhar, "Interference Mitigation in Turbo-Coded OFDM Systems Using Robust LLRs", IEEE ICC-08, pp. 646-651, 2008

[27] D. C. Brennan, "Linear diversity techniques", Proc. IRE, vol. 47, pp. 1075-1102, 1959

[28] A. Asadi and V. Mancuso, "WiFi direct and lte d2d in action," in Wireless Days (WD), 2013 IFIP, Nov 2013, pp.1-8

[29] B. Muquet, Z. Wang, G. B. Giannakis, M. de Courville, and P. Duhamel, "Cyclic Prefixing or Zero Padding for Wireless Multicarrier Transmission,"IEEE Transactions on Communications, vol.50 , December 2002

PUBLICATIONS

1. Vishnu OC, Vignesh Kumar, Midhun Madhusoodanan and K Giridhar, "Joint Uplink LLR Computation, Quantization, and Combining for Load-Balanced Small Cells", Submitted in March-2016 to IEEE GlobeComm.

2. Vishnu OC, V Vignesh Kumar, and K Giridhar ,"Robust Multiuser Detection for Coordinated Communication in UHF Band", Presented at WWRF-36, Beijing(China), May 2016

3. K. Giridhar, Suman Kumar, V. Vignesh Kumar, P. Sriram, C.R. Venkatesh, B. Arun Ayyar, O.C. Vishnu, M. Midhun, Umakishore G.S.V, B. Sendil Kumar, B. Naveen Kumar, Deepak Saidam,"Multi-Operator Simultaneously Shared Synchronised Air Interface for Communication", Submitted to IEEE-JSAC special issue on "Spectrum Sharing and Aggregation for Future Wireless Networks".

4. Vishnu OC, Vignesh Kumar, Midhun Madhusoodanan and K Giridhar, "Uplink LLR combining method for multioperator spectrum sharing", Provisional filed at Patent office, Guindy, Chennai with Ref No:IDF 1420